Astron. Astrophys. 271, 149–166 (1993)

ASTRONOMY AND ASTROPHYSICS

A model for the intrinsic population of cataclysmic variables

U. Kolb

Max-Planck-Institut für Astrophysik, Karl-Schwarzschild-Strasse 1, W-8046 Garching, Germany

Received November 26, accepted December 20, 1992

Abstract. Applying standard models of the formation and evolution of cataclysmic variables (CVs) we synthesize theoretically the present intrinsic CV population in a self-consistent way. This is done by combining published CV formation rates with a large number of evolutionary sequences covering all possible initial configurations. The influence of different assumptions entering the determination of the birth rate and of different prescriptions to compute magnetic braking is investigated quantitatively. As a main result we find that the detailed treatment of the common envelope phase has little influence, and that the most often cited prescriptions for magnetic braking give similar distributions. A theoretically predicted observable period histogram shows the principal effect of observational selection and proves that a pronounced "period gap" exists in the distribution of the total CV population when the disrupted magnetic braking model is applied to describe the evolution of individual CVs.

Key words: binaries:close – stars: evolution – novae, cataclysmic variables

1. Introduction

Cataclysmic variables (CVs) are short-period binaries consisting of a white dwarf (WD) primary and a low-mass main-sequence companion. The orbital distance is so small that the secondary fills its critical Roche volume and transfers matter through the inner Lagrangian point to the WD, which is – at least in the absence of a strong magnetic field – surrounded by an accretion disk (see e.g. Warner 1976). A possible evolutionary channel leading to such close systems involves a common envelope (CE) phase after a dynamically unstable mass transfer from a giant to an unevolved secondary (proposed for the first time by Paczyński 1976). After the spiralling-in and the ejection of the giant's envelope, the core of the giant (the later WD) and the more or less unaffected secondary form a close (but detached) pre-CV (see e.g. deKool 1992, hereafter DK). The transition to the semi-detached state of a CV and the subsequent long-term evolution in the CV phase with mass transfer from the secondary to the WD are both thought to be driven by orbital angular momentum losses $\dot{J}$, caused by gravitational radiation (GR; Kraft et al. 1962) and magnetic braking (MB; see e.g. Verbunt & Zwaan 1981). In particular, some peculiarities in the observed period distribution of CVs (the "period gap" between $\sim$ 2 h and $\sim$ 3 h, the "minimum period" at $\approx$ 80 min., see e.g. Ritter 1990; Fig. 1 of Ritter & Kolb 1992) lead to the disrupted magnetic braking model for the secular evolution of CVs (Spruit & Ritter 1983; Rappaport et al. 1983), where it is assumed that MB becomes abruptly ineffective when the secondary enters the fully convective state (for recent reviews see King 1988; Ritter 1991). Although the fundamental ideas about the formation and evolution of CVs were formulated for the first time several years ago, the presently discussed refined models still contain some poorly known parameters. As far as the evolution is concerned, these are mainly the functional dependence of the orbital angular momentum losses $\dot{J}_{\rm MB}$ due to magnetic braking on system parameters (in the following referred to as "MB law"), which up to now cannot be derived from first principles, and the possible time-dependence of the WD mass. A promising way to constrain such parameters involves the study of collective properties of CVs: the comparison of *observed* distributions of global system quantities (like orbital period P, WD mass M_1, secondary mass M_2) with the corresponding theoretically predicted *observable* distribution functions.

From the observational point of view, this requires the determination of system parameters for a large number of CVs. At present, the orbital period is known with sufficient precision for $\approx$ 200 systems; the components' masses are more difficult to measure and thus known with lower accuracy in general and for fewer systems (see e.g. Ritter 1990). Nevertheless, the steadily increasing number of publications reporting observational work on CVs shows that this situation is likely to improve in the near future.

On the other hand, in order to arrive at *theoretically* predicted observable distributions – which is the aim of our work – it is necessary to deal with a number of different problems, summarized and arranged in a logical sequence by the following three questions:

How many CVs form at a given time t and what initial configuration do they have? More precisely: If we define as a *generation* of CVs all those CVs born at the same time t (within a

certain time interval dt), the first problem consists of computing the distribution of each CV generation over a certain initial configuration space (in other words: to determine the birth rate).

How does a generation of CVs evolve? Each generation evolves, hence the present distribution of a generation today differs from its initial distribution. Superimposing the contributions of all generations which have been born since the formation of our galaxy yields the intrinsic distribution of the present population of CVs.

What fraction of the present population of CVs do we see? Taking into account observational selection effects transforms the intrinsic distribution into the (predicted) observable distribution, which can differ significantly.

The lack of any quantitative model of the formation rate and the impossibility to cover the whole initial configuration space by evolutionary sequences of CVs applying available computational tools — which would have required a tremendous amount of CPU-time — forced earlier work in this field to treat the problem with fairly crude approximations: Rappaport et al. (1983) tried to arrive at a predicted P-histogram for CVs — later also Hameury et al. (1990), but for AM Her stars only — based on a quantitatively insufficient bipolytrope description of the secular evolution. Both groups used only a few computed sequences and combined them with very simple assumptions about the birth rate and observational selection. The study of Ritter & Burkert (1986) concentrated on observational selection and relied on an even simpler treatment of CV evolution (where the secondary is assumed to be always in thermal equilibrium, i.e. a ZAMS star). Finally Shafter (1992) applied Politano's results describing the CV formation rate (Politano 1988), but restricted himself to the same simple treatment of the secular evolution as Ritter & Burkert (for a further comment on Shafter see Sect. 5).

The detailed computations of the CV birth rate performed by Politano (1988) and deKool (DK), together with the availability of the generalized bipolytrope model for the secondary to describe the secular evolution (Kolb & Ritter 1992; hereafter KR) enable us now to calculate for the first time a self-consistent and (within the approximations of the model) complete intrinsic CV population.

The emphasis of this paper is on the second of the questions formulated above: Section 2 solves the problem of transforming the known birth rates to the present day CV population and correcting for observational selection in a formal language. The actual numerical procedures for computing intrinsic distribution functions and the underlying physical models are explained in Sect. 3. The results – various intrinsic population models, computed using different sets of input parameters (birth rates, MB-laws) – are presented and compared in Sect. 4, where we also show the main effect of observational selection. A summary and discussion of important results and simplifications (Sect. 5) conclude this paper.

2. CV population synthesis: a formal approach

2.1. Determination of intrinsic distributions

We begin with a formal description of the problem to convert given CV birth rates into intrinsic distributions by means of the known secular evolution of CVs. The formalism is as general as possible to allow its application on various quantities and problems. The treatment of comparable problems in some former publications (Ritter & Burkert 1986; Ritter et al. 1991) is restricted to special circumstances and results naturally from our general description when applied to the situation in question (an example is discussed at the end of this paragraph).

Consider the m-dimensional configuration space $Q \subset \mathbb{R}^m$ defined by a set of m system quantities $Q_1, \ldots, Q_m$ (like WD mass, secondary mass, orbital period, ...). A CV is represented by the vector $\boldsymbol{q} = (q_1 \ldots q_m) \in Q$ consisting of the values q_i for the quantities Q_i in this system. The set Q_i should be *complete* with respect to a certain underlying CV-model in the sense that a newborn CV which appears in Q with a certain *initial* configuration $\boldsymbol{x} = (x_1 \ldots x_m) \in Q$ is unambiguously identified by $\boldsymbol{x}$ and the time $t \in [0, T_G] \subset \mathbb{R}$ of its birth. Here t is measured on a galactic time axis τ defined such that at $\tau = 0$ our galaxy has formed, and that T_G is its present age (i.e. $\tau = T_G$ denotes the present). The subsequent secular evolution changes the configuration of a CV and finally leads to the state $\boldsymbol{y} = (y_1 \ldots y_m) \in Q$ of the CV today (at $\tau = T_G$) – hereafter referred to as the *final* configuration.

More generally speaking, the secular evolution *maps* each initial configuration $(t, \boldsymbol{x})$ to the corresponding final configuration $\boldsymbol{y}$, i.e. defines a mapping

$$ev : \mathbb{R} \times Q \longrightarrow Q, \quad (t, \boldsymbol{x}) \longmapsto \boldsymbol{y}\,. \tag{1}$$

The differential CV formation rate $b(t, \boldsymbol{x})$ measuring the number density of systems (per pc^3 in the galactic mid-plane) forming at $\tau = t$ with the initial configuration $\boldsymbol{x}$, per time interval dt and intervals d$x_1, \ldots,$ dx_m, can be interpreted as a distribution function on $\mathbb{R} \times Q$,

$$b : \mathbb{R} \times Q \longrightarrow \mathbb{R}, \quad (t, \boldsymbol{x}) \longmapsto b(t, \boldsymbol{x})\,, \tag{2}$$

describing the *initial state* of the whole CV population. At present ($\tau = T_G$) the latter consists of

$$n_\Sigma = \int_0^{T_G} \int_Q b(t, \boldsymbol{x})\, \mathrm{d}x_1 \ldots \mathrm{d}x_m\, \mathrm{d}t \tag{3}$$

systems per pc^3 in the galactic mid-plane. The mapping ev transforms the distribution b into a new distribution n,

$$n : Q \longrightarrow \mathbb{R}, \quad \boldsymbol{y} \longmapsto n(\boldsymbol{y})\,, \tag{4}$$

describing the *final state* of the CV population — or, in other words, the *intrinsic distribution* of the present population of CVs.

To perform this transformation we consider an extension of ev, the mapping f

$$f : \mathbb{R} \times Q \longrightarrow \mathbb{R} \times Q \qquad (t, \boldsymbol{x}) \longmapsto (z, \boldsymbol{y}) , \tag{5}$$

where the additional variable z has to be chosen in such a way that f is a one-to-one transformation, i.e. that the inverse mapping f^{-1} exists and that f is differentiable (in the following we shall assume that the mapping ev and the quantities Q_i are such that an invertible and differentiable mapping like f always exists). Locally, in the vicinity of $(t_0, \boldsymbol{x}_0)$, f can be approximated by the Jacobian matrix $J_f(t_0, \boldsymbol{x}_0)$:

$$\mathbf{J}_f(t_0, \boldsymbol{x}_0) = \begin{pmatrix} \frac{\partial z}{\partial t} & \frac{\partial z}{\partial x_1} & \cdots & \frac{\partial z}{\partial x_m} \\ \frac{\partial y_1}{\partial t} & \frac{\partial y_1}{\partial x_1} & \cdots & \frac{\partial y_1}{\partial x_m} \\ \vdots & \vdots & \ddots & \vdots \\ \frac{\partial y_m}{\partial t} & \frac{\partial y_m}{\partial x_1} & \cdots & \frac{\partial y_m}{\partial x_m} \end{pmatrix}_{(t_0, x_0)} . \tag{6}$$

Thus f maps the volume element $\mathrm{d}V_Q = \mathrm{d}t\,\mathrm{d}x_1 \ldots \mathrm{d}x_m$ surrounding the point $(t_0, \boldsymbol{x}_0)$ to a volume element – containing the image $(z_0, \boldsymbol{y}_0)$ – of size

$$\mathrm{d}V'_Q = \mathrm{d}z\,\mathrm{d}y_1 \ldots \mathrm{d}y_m = |\det \mathbf{J}_f|_{(t_0, x_0)}\,\mathrm{d}V_Q . \tag{7}$$

If $\tilde{n}$ denotes the distribution of the final state of the CV population in the extended configuration space $\mathbb{R} \times Q$, i.e. the distribution resulting when b is transformed by the mapping f, then the number of systems (per pc^3) in $\mathrm{d}V_Q$ and mapped to $\mathrm{d}V'_Q$ is

$$\mathrm{d}n_\Sigma = b(t_0, \boldsymbol{x}_0)\,\mathrm{d}V_Q = \tilde{n}(z_0, \boldsymbol{y}_0)\,\mathrm{d}V'_Q . \tag{8}$$

Using Eq. (7) this can be solved for $\tilde{n}$:

$$\tilde{n}(z, \boldsymbol{y}) = \left.\frac{b}{|\det \mathbf{J}_f|}\right|_{f^{-1}(z,y)} , \tag{9}$$

where the right hand side has to be taken at $f^{-1}(z, \boldsymbol{y}) = (t, \boldsymbol{x})$, i.e. at the pre-image of $(z, \boldsymbol{y})$ with respect to f. Finally, the m-dim. distribution function n results from $\tilde{n}$ by integrating over the additional variable z:

$$n(\boldsymbol{y}) = \int \tilde{n}(z, \boldsymbol{y})\,\mathrm{d}z . \tag{10}$$

An obvious choice for z is the formation time t itself. With $z \equiv t$ the Jacobian of Eq. (6) simplifies to

$$\det \mathbf{J}_f(t_0, \boldsymbol{x}_0) = \left.\frac{\partial(\boldsymbol{y})}{\partial(\boldsymbol{x})}\right|_{(t_0, x_0)} , \tag{11}$$

and Eq. (10) reads

$$n(\boldsymbol{y}) = \int_0^{T_G} \left.\frac{b}{|\partial(\boldsymbol{y})/\partial(\boldsymbol{x})|}\right|_{f^{-1}(t,y)} \mathrm{d}t . \tag{12}$$

Let us now apply this formalism to a simple evolutionary model: If the newborn CV is completely characterized by the initial values for the WD and secondary mass, $M_{1,\mathrm{i}}$ and $M_{2,\mathrm{i}}$ (see below, Sect. 3.1), and if further the secular mean of the WD mass remains constant throughout the evolution (as it is the case if the binary loses all the transferred matter during nova explosions), then $M_{2,\mathrm{i}}$ is a useful supplementary variable. With $\boldsymbol{x} = (M_{1,\mathrm{i}}, M_{2,\mathrm{i}})$, $\boldsymbol{y} = (M_1, M_2)$ and $z \equiv M_{2,\mathrm{i}}$ the Jacobian of Eq. (6) simply reduces to the derivative $-\partial M_2/\partial t < 0$, evaluated at the pre-image of $(M_{2,\mathrm{i}}, M_1, M_2)$, and thus is equal to the mass transfer rate $+\dot{M}_2 = \dot{M}_2(M_{2,\mathrm{i}}, M_{1,\mathrm{i}}, M_2) < 0$ in a CV which has the secondary mass M_2 and was born with $(M_{1,\mathrm{i}}, M_{2,\mathrm{i}})$.

To understand this consider a CV with present secondary mass M_0, (constant) WD mass M_1, and born at $\tau = t_0$ with $M_{2,\mathrm{i}} = M_{\mathrm{i},0}$. Let $\tilde{\tau}$ denote the system's age, i.e. today $\tilde{\tau} = \tilde{t}_0 = T_G - t_0$. A change of t_0 to $t_0 + \mathrm{d}t$ (but with fixed $M_{\mathrm{i},0}$) changes the present secondary mass from M_0 to $M_0 + \mathrm{d}M_2$ and is equivalent to the change of the present system age from $\tilde{t}_0$ to $\tilde{t}_0 - \mathrm{d}t$, which also leads to the new secondary mass $M_0 + \mathrm{d}M_2$. Thus

$$\begin{aligned} -\left.\frac{\partial M_2}{\partial t}\right|_{f^{-1}(M_{\mathrm{i},0}, M_1, M_0)} &= \frac{\mathrm{d}M_2}{\mathrm{d}\tilde{\tau}}\,(M_{\mathrm{i},0}, M_1, M_0) \\ &= \dot{M}_2\,(M_{\mathrm{i},0}, M_1, M_0) . \end{aligned} \tag{13}$$

The same interpretation is possible for all derivatives $\partial y_i/\partial t$ in the Jacobian matrix Eq. (6).

Accordingly, in our simple example the intrinsic distribution is given by

$$n(M_1, M_2) = \int_{M_2}^{M_{2,\max}} \frac{b|_{f^{-1}(M_{2,\mathrm{i}}, M_1, M_2)}}{|\dot{M}_2(M_{2,\mathrm{i}}, M_1, M_2)|}\,\mathrm{d}M_{2,\mathrm{i}} , \tag{14}$$

where the integration bounds derive from the requirement $M_{2,\mathrm{i}} > M_2$ and from the stability criterion for mass transfer in CVs ($M_{2,\mathrm{i}} < M_{2,\max}$, see Sect. 3.1). Equation (14) is equivalent to Eq. (6) of Ritter & Burkert (1986), where, however, $\dot{M}_2$ is assumed to be independent of $M_{2,\mathrm{i}}$ and thus outside the integral.

2.2. *Observable distributions*

The intrinsic distribution $n(\boldsymbol{y})$ computed in the previous paragraph is a distribution function of the CV number density n per pc^3 in the galactic mid-plane. In contrast, the predicted observable distribution $N(\boldsymbol{y})$ has to be a distribution of the total number of observable CVs. Both, n and N, are connected by a volume integration in the real, physical space:

$$N(\boldsymbol{y}) = \int_{V(y)} n(\boldsymbol{y})\,d(h)\,\mathrm{d}V =: n(\boldsymbol{y})\,s(\boldsymbol{y}) . \tag{15}$$

Here the function $d(h)$ describes the dependence of the CV number density on the distance h from the galactic mid-plane, e.g.

$$d(h) = \exp\left\{-\frac{1}{2}\left(\frac{h}{H_{\rm CV}}\right)^2\right\} \tag{16}$$

with a typical scale height $H_{\rm CV}$ on order of 200 – 300 pc, see Ritter & Burkert (1986). The volume $V(\boldsymbol{y})$ is determined by the maximum distance $r_{\rm max}$ up to which CVs with a configuration $\boldsymbol{y}$ (i.e. a certain luminosity) can be detected. Clearly, $r_{\rm max}$ depends in general on $\boldsymbol{y}$ and on the direction of observation — $V(\boldsymbol{y})$ is not just a sphere. As is obvious from Eq. (15), the observable distribution $N(\boldsymbol{y})$ can be obtained from $n(\boldsymbol{y})$ by a simple multiplication with the differential selection factor $s(\boldsymbol{y})$, which contains the whole information about observational selection.

3. The numerical model

In the following, we briefly describe the birth rate models which serve as an input for our study, the simplifying assumptions about the secular evolution of CVs, and the numerical realization of the concepts introduced in the previous section — a procedure finally leading to a self-consistent intrinsic CV population model.

3.1. Formation of CVs, birth rates

Up to now, the only available computations of a differential CV formation rate were performed by Politano (1988; for a short description see also Politano 1990; Ritter et al. 1991) and deKool (DK). Both studies rely on the same analytical fits to results from calculations of single star evolution on an extended grid of stellar masses. Assuming a (constant) total star formation rate and certain initial distributions for orbital distance, primary mass and mass ratio q_0 in main-sequence binaries (where both components are ZAMS stars) lead the authors then to a quantitative determination of the outcome of the evolutionary channel generating CVs. As usual, the complex CE-phase involved was described by a single parameter $\alpha_{\rm CE}$, measuring the efficiency of envelope ejection, thus fixing the orbital separation of the remaining close CV precursor. Subsequent operation of magnetic braking (only if the secondary is not fully convective) and gravitational radiation was assumed to drive a system into contact (for a full description of the input physics see Politano 1988 and DK).

The prehistory of a newborn CV is generally short compared to the nuclear timescale of the secondary, so we neglect effects of nuclear evolution and assume that the secondary is initially chemically homogeneous (with a standard Population I mixture, $X = 0.70$, $Z = 0.02$) and in thermal equilibrium. Accordingly, the initial configuration of a CV is completely described by the initial WD mass $M_{1,\rm i}$ and the initial secondary mass $M_{2,\rm i}$ (or, equivalently, the initial mass ratio $q_{\rm i} = M_{1,\rm i}/M_{2,\rm i}$) – via the mass-radius relation for ZAMS stars, Roche geometry and

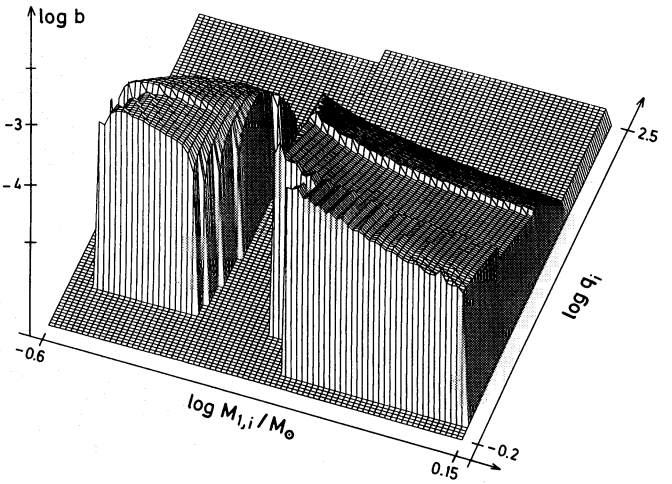

Fig. 1. Surface plot depicting the CV birth rate $\log b(\log M_{1,\rm i}, \log q_{\rm i})$ computed by Politano (1988) as a function of the initial WD mass $M_{1,\rm i}$ and the initial mass ratio $q_{\rm i} = M_{1,\rm i}/M_{2,\rm i}$, in arbitrary normalization. There are two ridges visible along lines of constant secondary mass ($M_{2,\rm i} = 0.37M_\odot$ and $M_{2,\rm i} = 0.085M_\odot$); both are purely numerical and indicate the onset of magnetic braking and the low-mass end of the ZAMS, respectively

Kepler's third law. We furthermore assume for simplicity that the CV formation rate b was at any time the same as at present, i.e.

$$\partial b/\partial t = 0\ ;\ b(t, \boldsymbol{x}) = b(T_{\rm G}, \boldsymbol{x})\ ;\ \boldsymbol{x} = (M_{1,\rm i}, M_{2,\rm i})\ . \tag{17}$$

As an example, Fig. 1 shows model Pol (see Table 1), the formation rate as computed by Politano (1988). The two most remarkable features – both leaving signatures in the resulting CV population models to be discussed below – of such a distribution of newborn CVs are: a) the separation into two distinct groups comprising the systems with low-mass He-WDs ($M_{1,\rm i} \lesssim 0.46M_\odot$) and high-mass C/O-WDs ($M_{1,\rm i} \gtrsim 0.51M_\odot$; O/Ne/Mg-WDs are not considered separately); b) the fact that for a given $M_{1,\rm i}$ the birth rate is largest in the vicinity of the maximum possible value $M_{2,\rm max}$ for $M_{2,\rm i}$.

The gap in $M_{1,\rm i}$ is a relic of the binary's prehistory and reflects the difference between the core mass (the later WD mass) of a primary which succeeds in filling its Roche lobe for the first time just before the onset of He-burning, and of a primary which is slightly too small at that time, thus filling its Roche lobe not until the beginning of its AGB phase (see e.g. DK). The maximum mass $M_{2,\rm max}$, on the other hand, is due to stability requirements for the mass transfer in CVs, which can be approximated by

$$\frac{M_{1,\rm i}}{M_{2,\rm i}} > q_{\rm crit} \approx \begin{cases} 0.8 & \text{for } M_{2,\rm i} > 0.8M_\odot \\ 1.5 & \text{for } M_{2,\rm i} \le 0.8M_\odot \end{cases} \tag{18}$$

(e.g. Politano 1988). To provide a smooth transition of $q_{\rm crit}$ in the regime $0.5 \lesssim M_{2,\rm i}/M_\odot \lesssim 0.8$ Politano improved this simple criterion according to calculations performed by Hjellming

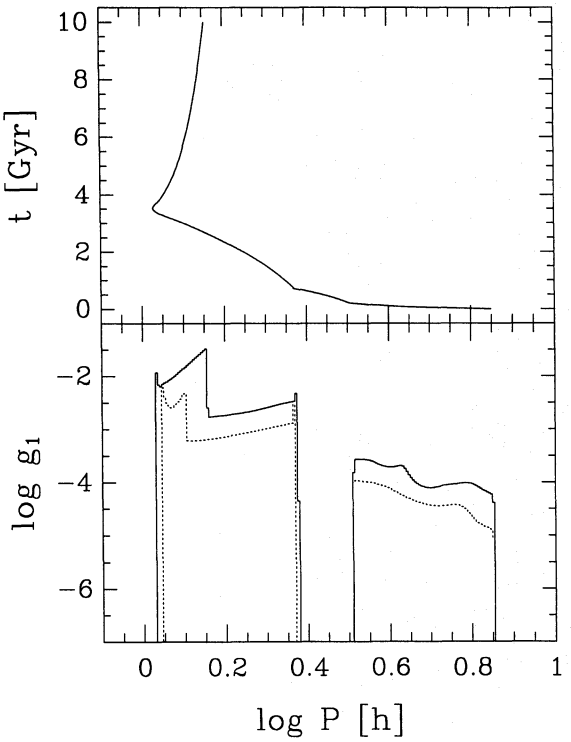

Fig. 2. *Upper frame:* The secular evolution of a CV born with $M_{1,i} = 1.0M_\odot$, $M_{2,i} = 0.9M_\odot$, computed with the bipolytrope code and assuming the MB-law VZtotal (see Table 2). Plotted is the system's age t (in 10^9 yr) as a function of orbital period (in h). *Lower frame:* The corresponding distribution function $g_1(\log P)$ as defined in Eq. (29) for the sequence shown in the upper frame (full line), and for a corresponding sequence computed with a full stellar evolution code (sequence no. 1 of KR; dotted), both in arbitrary normalization. Systems in the detached phase do not contribute to g_1

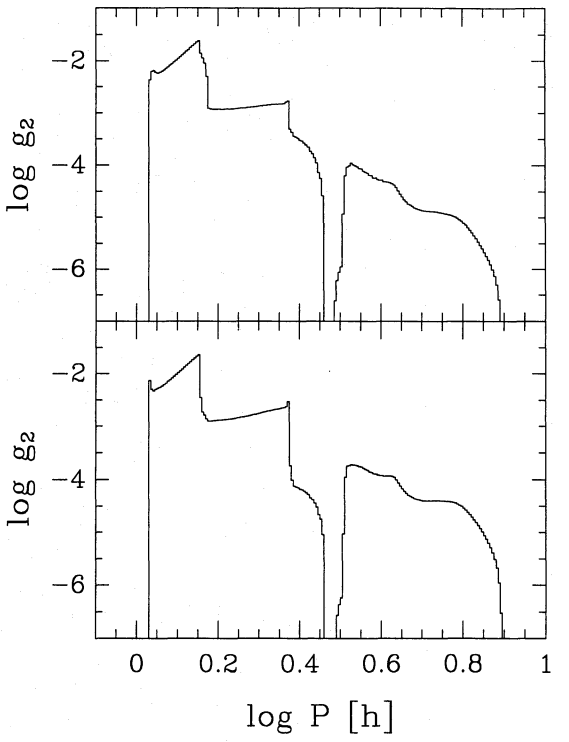

Fig. 3. The distribution function $g_2(\log P)$, defined in Eq. (30), for $M_{1,i} = 1.0M_\odot$, $0.1 \leq M_{2,i}/M_\odot \leq 1.0$, MB-law VZtotal, assuming the formation rate model bConst (upper frame) and Pol (lower frame). The normalization is arbitrary

Furthermore, if the formation rate b does not depend on t (as it is assumed in our study, see Sect. 3.1), then $g_1(\log P)$ is proportional to the slope of the graph (or, more precisely, to the sum of the slopes over all branches of the graph) in a diagram where the age of a CV born with $(M_{1,i}, M_{2,i})$ is plotted as a function of $\log P$ (see Fig. 2). This is also obvious from physical arguments: a high "velocity" $|\dot{P}|$ in period space is equivalent to a low occupation probability

$$g_1(\log P) \propto \frac{1}{|\mathrm{d}\log P/\mathrm{d}t|} \propto \frac{P}{|\dot{P}|} \tag{29}$$

in a given period bin.

As an example Fig. 2 plots in the upper frame the relation $t(\log(P/\mathrm{h}))$ for an evolutionary sequence computed with the bipolytrope code, and in the lower frame (full line) the resulting distribution $g_1(\log P)$, adopting an arbitrary value for $b(M_{1,i}, M_{2,i})$. The dotted line represents sequence no. 1 of KR, obtained with Mazzitelli's full stellar evolution code, and proves once again the satisfying overall agreement between results of a full stellar evolution computation and the calibrated bipolytrope approximation. The logarithmic scale for g_1 allows to account for the difference in evolutionary time scales above and below the period gap.

By comparing the upper and lower frame of Fig. 2 the main features of $g_1(\log P)$ become immediately obvious: the "spikes" at the minimum period and at turn-on of mass transfer below the period gap (in both cases $\dot{P} = 0$, hence $g_1(\log P) \to \infty$; due to the finite resolution of the histogram in Fig. 2 the g_1-value remains finite); and the step at $\log(P/\mathrm{h}) \approx 0.15$, characterizing the end of the evolutionary sequence after arriving at an age of 10^{10} yr. The computation with the full stellar evolution code was pursued only up to an age of $5.5\ 10^9$ yr, so that the corresponding step in g_1 is at a lower P. Above the period gap one has to be careful when interpreting the detailed structure of $g_1(\log P)$: the local maximum at $\log(P/\mathrm{h}) \approx 0.63$ is a numerical artefact of the bipolytrope description, caused by the transition of the central polytropic index cpn from the steep part of the calibration curve $cpn(M_2)$ to the asymptotic flat part for small M_2 (see Fig. 5 in KR). This transition manifests itself also as a local maximum of the mass transfer rate in sequences computed with the bipolytrope code, a feature not present in the corresponding sequences computed with a full stellar evolution code (see e.g. Figs. 8 and 9 in KR, at $P/\mathrm{h} \approx 4.5$ and at $\log(t/\mathrm{yr}) \approx 7.8$, respectively).

Figure 3 shows the distribution

$$g_2(\log P) = \int \tilde{n}(\log P, M_{1,0}, M_{2,i})\,\mathrm{d}M_{2,i}\ , \tag{30}$$

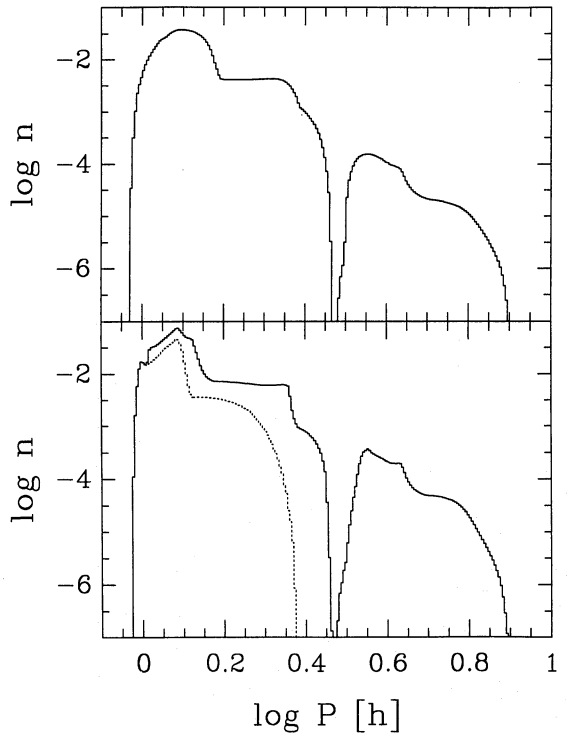

Fig. 4. The intrinsic period distribution $n(\log P)$ for models pm1 (upper frame) and pm3 (lower frame), see Table 3. The dotted line in the lower frame shows the contribution of CVs with He-WDs. The function n results from a superposition of the subdistributions $g_2(\log P)$ for all possible values of $M_{1,i}$ (see Fig. 3) and is not normalized

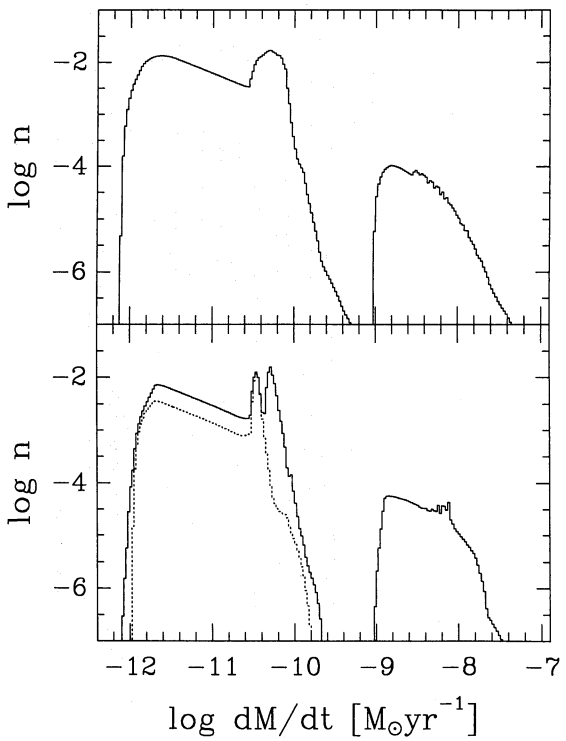

Fig. 5. The intrinsic distribution function $n(\log \dot{M})$ of the mass transfer rate $\dot{M} = |\dot{M}_2|$ (in $M_\odot \mathrm{yr}^{-1}$) for models pm1 (upper frame) and pm3 (lower frame), see Table 3, not normalized. The dotted line in the lower frame shows the contribution of CVs with He-WDs

i.e. the superposition of all subdistributions $g_1(\log P)$ belonging to a fixed value $M_{1,i} = M_{1,0}$, but to different initial secondary masses, assuming the formation rate model bConst (upper frame) and Pol (lower frame). The "period gap" of g_1 between $\log(P/\mathrm{h}) \approx 0.37$ and ≈ 0.51 due to systems in the detached phase is now partly filled up by young systems, which are born in this period interval and still located there. However, for $\log(P/\mathrm{h}) > \log(P_{\mathrm{crit}}/\mathrm{h}) = 0.4675$ the gap population is much smaller than for $\log(P/\mathrm{h}) \leq 0.4675$, because secondaries with initially small radiative cores react like their fully convective counterparts in adiabatic response to mass transfer with an initial expansion, leading to an increase of the orbital period until thermal relaxation restores the usual secular trend $\dot{P} < 0$. The extent of the excursion towards longer P is roughly proportional to the angular momentum loss rate (for a detailed discussion see Ritter & Kolb 1992) and thus larger by a factor ~ 20 for $\log(P/\mathrm{h}) > 0.4675$ — actually so large that CVs leave the interval $0.47 \lesssim \log(P/\mathrm{h}) \lesssim 0.51$ within only $\sim 10^7$ yr towards longer periods, hence keeping this region "clear" of systems (see Fig. 8, and also Fig. 2 of KR).

Finally, Fig. 4 depicts the period distribution $n(\log P)$ of the total present CV population (within the restrictions and simplifications of Sect. 3), i.e. the superposition of all subdistributions $g_2(\log P)$ for all possible WD masses, assuming the formation rate prescription bConst (upper frame; model pm1) and Pol (lower frame; model pm3), see Table 3. The distribution of model pm1 is clearly smoother than the one of pm3; that is simply because in the former all CVs contribute with equal strength, whereas in the latter systems born with the highest possible secondary mass dominate (see Sect. 3.1), so that structures in the corresponding subdistributions are preserved in $n(\log P)$. The general increase of n towards shorter orbital periods also has a simple explanation: only very young CVs born with high P-values populate the region of the longest periods; towards shorter periods one finds not only the young CVs born there, but also older systems descending from longer periods. The local maximum of $g_1(\log P)$ at $\log(P/\mathrm{h}) \approx 0.63$ (see above) is not smeared out in the total distribution n, since all subdistributions extending beyond $\log(P/\mathrm{h}) = 0.63$ show this numerical artefact at almost the same period. As Fig. 4 shows a pronounced "intrinsic period gap" restricts itself to the interval $0.47 \lesssim \log(P/\mathrm{h}) \lesssim 0.50$, although the period range of the detached phase of CVs born with high initial secondary masses, $0.37 \lesssim \log(P/\mathrm{h}) \lesssim 0.51$ (see Fig. 2; the borders depend slightly on the WD mass), is still visible.

4.2. The intrinsic distribution of mass transfer rates

The analysis of the period distribution outlined in the previous paragraph can be applied in a similar way to the distribution of mass transfer rates $\dot{M}$. The results of such a population synthe-

Table 1. Parameters of the different CV formation rate models

model	$b_\Sigma/\mathrm{pc}^{-2}\mathrm{yr}^{-1}$	$\alpha_{\rm CE}$	q_0-distribution	remarks
Pol	$1.05 \cdot 10^{-12}$	1	$q_0 = 1$ strongly preferred	
dK1	$3.70 \cdot 10^{-12}$	1	$q_0 = 1$ preferred	
dK1in	$11.5 \cdot 10^{-12}$	1	independent choice	
dK03in	$8.77 \cdot 10^{-12}$	0.3	independent choice	
bConst	-	-	-	$b(\log M_{1,\rm i}, \log M_{2,\rm i}) = \text{const.}$
M2max	-	-	-	$b(\log M_{1,\rm i}, \log M_{2,\rm i}) = b_0 \delta(\log M_{2,\rm i} - \log M_{2,\max})$

(1989) when computing model Pol (Politano, private communication).

A different computational technique (a Monte Carlo approach) enabled deKool to investigate easily the influence of various parameters on the CV formation rate; therefore, we have available three more models for $b(M_{1,\rm i}, M_{2,\rm i})$, namely dK1, dK1in and dK03in (see Table 1), which are the "standard models" 1, 3, and 4 defined in DK, apart from the fact that the original MB-law according to Verbunt & Zwaan (1981) was applied (deKool, private communication) — instead of the modified version used in DK and in Politano (1988).

In particular, these additional birth rate models allow the investigation of the influence of $\alpha_{\rm CE}$ ($\alpha_{\rm CE} = 1$ in dK1in, $\alpha_{\rm CE} = 0.3$ in dK03in) and of the q_0-distribution (a strong preference of $q_0 = 1$ in dK1, and the independent choice of primary and secondary mass in the main-sequence binary from the same mass function in dK1in). Model dK1 is similar to model Pol (where the preference of $q_0 = 1$ is even stronger) and yields, apart from the normalization, no significant difference in the resulting intrinsic CV populations.

We complete the set of birth rate distributions by two artificial, extreme cases: model bConst assumes a constant value for $b(\log M_{1,\rm i}, \log M_{2,\rm i})$, i.e.

$$\frac{\partial b}{\partial \log M_{1,\rm i}} = 0\,, \quad \frac{\partial b}{\partial \log M_{2,\rm i}} = 0 \tag{19}$$

for $-0.6 \le \log M_{1,\rm i}/M_\odot \le 0.15$ and $0.1 \le M_{2,\rm i}/M_\odot \le M_{2,\max}$ ($b = 0$ elsewhere), whereas in model M2max all CVs are thought to be born with the largest possible secondary mass $M_{2,\max} = M_{1,\rm i}/q_{\rm crit}$ allowed by the stability criterion (18), i.e.

$$\frac{\partial b}{\partial \log M_{1,\rm i}} = 0\,, \quad b(\log M_{1,\rm i}, \log M_{2,\rm i}) \propto \delta(\log M_{2,\rm i} - \log M_{2,\max}). \tag{20}$$

Table 1 summarizes our 6 birth rate models and the main input parameters in which they differ. The second column lists the total birth rate

$$b_\Sigma = \int\int b(M_{1,\rm i}, M_{2,\rm i})\, \mathrm{d}M_{2,\rm i}\, \mathrm{d}M_{1,\rm i} \tag{21}$$

as a surface number density of CV systems, i.e. the number density integrated perpendicular to the galactic plane. The original data of deKool consisted of CV number densities in the galactic mid-plane; we used Eq. (16) with $H_{\rm CV} = 250$ pc to obtain the value b_Σ in Table 1 (however, note that we don't make use of b_Σ in our purely differential study).

3.2. *Secular evolution*

The different birth rate models serve as an important input for our CV population synthesis. They are combined with computations of the secular evolution of CVs in the following way: Instead of solving the integral Eq. (10) we explicitly execute the mapping ev defined in Eq. (1) by covering the 2-dim. initial configuration space with a mesh $(M_{1,\rm i}, M_{2,\rm i})_{jk}$ and computing for each grid point the corresponding secular evolution. In view of CPU-time limitations, the large number of evolutionary sequences required can be achieved only if a simplified model for the secular evolution is applied. The generalized bipolytrope model for the secondary (see KR for any details) proves to be a suitable tool: calibrated to a full stellar evolution code (in our case Mazzitelli's code, see e.g. Mazzitelli 1989) it succeeds in reproducing the time evolution of all quantities of interest for our study with an accuracy $\lesssim 5\%$ when compared to results obtained with the full code (for an extended discussion of the limtations of the bipolytrope model see KR). Unfortunately, it is not possible to treat high-mass secondaries ($\gtrsim 1 M_\odot$) within the bipolytrope approximation, mainly because for these the convective envelope becomes too small (see KR). Accordingly, the coverage of the initial configuration space is restricted to systems with $M_{2,\rm i} \le 1.0 M_\odot$ and we miss $\sim 20\%$ of the total CV population (see Sect. 5).

The adopted calibration of the bipolytrope code (the same as in KR) leads to the value $M_{\rm conv,0} = 0.3655 M_\odot$ for the limiting stellar mass where ZAMS models become fully convective. A CV with this secondary mass would turn on mass transfer at the "critical" orbital period $\log(P_{\rm crit}/\mathrm{h}) = 0.4675$.

Magnetic braking $\dot J_{\rm MB}$ is assumed to operate only in case of secondaries with a radiative core, otherwise we use gravitational radiation as the only sink of orbital angular momentum. We investigate the influence of the MB-law by applying four different prescriptions (summarized in Table 2): the semi-empirical approaches according to Verbunt & Zwaan (1981) and according to Mestel & Spruit (1987; see also Hameury et al. 1988) with the values $f_{\rm VZ} = 1$ and $n_{\rm MS} = 1.2$, $p_{\rm MS} = 1$ for the free parameters, respectively, a modified Verbunt & Zwaan law where only the convective envelope's moment of inertia enters (instead of that of the whole star, see Eq. (2) of KR), and an artificial case with $\dot J/J = \text{constant}$.

Again for simplicity (and subject to future generalizations), we keep M_1 constant throughout the evolution, assuming that the system loses all the transferred matter during nova-explosions with the WD's specific orbital angular momentum

Table 2. Parameters of the different MB laws

model	free parameters	reference
VZtotal	$f_{\rm VZ} = 1$, $r_{\rm g} = r_{\rm g,total}$	Verbunt & Zwaan 1981
VZconv	$f_{\rm VZ} = 1$, $r_{\rm g} = r_{\rm g,conv}$	Eq. (2) in KR
MS	$n_{\rm MS} = 1.2$, $p_{\rm MS} = 1.0$	Mestel & Spruit 1987; Hameury et al. 1988
JConst		$(\dot J/J) = -5.7 \cdot 10^{-9}{\rm yr}^{-1}$

(observations and nova theory tend indeed to favour $\langle \dot M_1 \rangle \approx 0$, see e.g. Hameury et al. 1989 and Sect. 5) — equivalent to $\eta = 0$, $\nu = M_2/M_1$ in Eqs. (3) and (4) of KR.

The mesh covering the initial configuration space consists of $\sim 50 \times 200$ equidistant grid points in the direction of $M_{1,\rm i}$ and $M_{2,\rm i}$, respectively. For each grid point we computed the secular evolution of the corresponding newborn CV up to an age of $T_{\rm G} = 10^{10}$ yr and stored all essential quantities of the evolutionary sequence in a table comprising 200 – 400 time grid points, distributed according to evolutionary requirements. Each entry in such a table belongs to a certain system age $\tilde t$ and can be interpreted as the final (i.e. present) configuration of a CV born at time $t = T_{\rm G} - \tilde t \in [0, T_{\rm G}]$, contributing to the intrinsic distribution n with the weight $b(M_{1,\rm i}, M_{2,\rm i})$. From this data set we explicitly record n as a function of the variables $\boldsymbol{y} = (\log M_1, \log M_2, \log P, \log \dot M)$, i.e. n is a 4-dim. distribution function ($\dot M := |\dot M_2|$ denotes the mass transfer rate). Any subdistribution, e.g. the period distribution, can be obtained by a simple integration over the remaining variables. The specific choice for $\boldsymbol{y}$ is such that the inclusion of observational selection effects is as easy as possible.

3.3. Observational selection

Although we refrain from discussing any detailed model of observational selection, we wish to demonstrate its principal implications. For that purpose we consider the simplest conceivable model: a magnitude limited sample taken from a CV population which is uniformly distributed in physical space. The maximum distance up to which a system can be observed from earth is assumed to be determined by its bolometric accretion luminosity

$$L_{\rm acc} = -\frac{G M_1 \dot M_2}{R_1} \tag{22}$$

(R_1 is the WD's radius, G the constant of gravitation); the observable volume then scales with $L_{\rm acc}^{3/2}$.

Accordingly, we will show below (Sect. 4.5) a predicted observable CV distribution $N(\boldsymbol{y})$ computed with

$$s(\boldsymbol{y}) \propto \left(\frac{M_1}{R_1}|\dot M_2|\right)^{3/2} \tag{23}$$

for the differential selection factor s defined in Eq. (15).

4. Results: a comparison of population models

This section presents the resulting intrinsic CV "population models" (designated by "pm$j$", where $j = 1, \ldots, 9$, see Table 3, Sect. 4.4) for different combinations of the parameters introduced in Sect. 3.

To facilitate the following descriptions, we will refer to systems passing their intermediate phase without mass transfer subsequent to the secondary's transition to the fully convective state as "systems in the detached phase". Note that these are *not* CVs, since the latter are semi-detached by definition. Moreover, we denote the period at which a system enters and leaves the detached phase by $P_{\rm u}$ and $P_{\rm l}$, respectively.

A qualitative understanding of the intrinsic distribution functions is best provided by means of a step by step synthesis of the intrinsic period histogram, as demonstrated in the next paragraph.

4.1. The intrinsic period distribution

For a slightly different application of the formalism developed in Sect. 2 we define the mapping

$$\begin{aligned} f \;:\; & I \longrightarrow F \\ & (t, M_{1,\rm i}, M_{2,\rm i}) \longmapsto (P, M_{1,\rm i}, M_{2,\rm i}) \end{aligned} \tag{24}$$

from an initial configuration space I (with the variables t, $M_{1,\rm i}$ and $M_{2,\rm i}$) to the final configuration space F, consisting of P, $M_{1,\rm i}$ and $M_{2,\rm i}$, where P is the present period of a CV born with initial masses $M_{1,\rm i}$, $M_{2,\rm i}$ at $t \in [0, T_{\rm G}]$. With regard to $M_{1,\rm i}$ and $M_{2,\rm i}$ the mapping f is just the identity. Since a specific CV may cross the same period P twice (e.g. after passing the minimum period, or during the phase of turn-on of mass transfer, when thermal relaxation supersedes the initial adiabatic response of the secondary, see KR), f is *not* invertible. Nevertheless, f can be reduced to a finite number $L \in \mathbb{N}$ of branches f_l, defined on certain subsets $I_l \subset I$ of the initial space I:

$$f_l \;:\; I_l \subset I \longrightarrow F\,, \quad l = 1, \ldots, L\,. \tag{25}$$

Each f_l is invertible, and the sum over all branches f_l restores the original mapping f. Following the ideas of Sect. 2 and taking into account the Jacobian

$$\det \mathbf{J}_{f_l}(t_0, M_{1,\rm i}, M_{2,\rm i}) = \left.\frac{\partial P}{\partial t}\right|_{(t_0, M_{1,\rm i}, M_{2,\rm i})} \tag{26}$$

of f_l in $(t_0, M_{1,\rm i}, M_{2,\rm i})$ we obtain for the period distribution $n(P)$

$$n(P) = \int\int \tilde n(P, M_{1,\rm i}, M_{2,\rm i})\, {\rm d}M_{1,\rm i}\, {\rm d}M_{2,\rm i}\,, \tag{27}$$

where

$$\tilde n(P, M_{1,\rm i}, M_{2,\rm i}) = \sum_l \left.\frac{b}{|\partial P/\partial t|}\right|_{f_l^{-1}(P, M_{1,\rm i}, M_{2,\rm i})}\,. \tag{28}$$

Thus, if the subdistribution $g_1(\log P) := \tilde n(\log P, M_{1,\rm i}, M_{2,\rm i})$ is considered as a function of $\log P$ for a given set $(M_{1,\rm i}, M_{2,\rm i})$, the P-distribution $n(\log P)$ can be interpreted as the superposition of all subdistributions $g_1(\log P)$ for all possible sets of initial values $(M_{1,\rm i}, M_{2,\rm i})$.

sis for models pm1 and pm3 are shown in the upper and lower frames of Fig. 5, respectively. The distribution falls clearly into two parts, one with high and one with low $\dot{M}$-values — reflecting the different time scales of orbital angular momentum losses (which drive the mass transfer) of systems above and below the period gap. The "ripples" showing up in the region $-8.5 \lesssim \dot{M}/M_\odot \mathrm{yr}^{-1} \lesssim -8.0$ are again related to the property of the bipolytrope description leading to a local maximum $\dot{M}_{\max}$ of the mass transfer rate in evolutionary sequences around the orbital period $P/\mathrm{h} \approx 4.5$ (Fig. 8 of KR). Accordingly, the corresponding subdistributions $g_1(\log \dot{M}) \propto |\dot{M}/\ddot{M}|$ grow to infinity at $\dot{M} = \dot{M}_{\max}$ ($\ddot{M} = 0 \Rightarrow g_1 \to \infty$).

On the other hand, the broad absolute maximum of $n(\log \dot{M})$ for model pm1 at $\log(\dot{M}/M_\odot \mathrm{yr}^{-1}) \approx -10.3$ is real and belongs to CVs located below the period gap, but still above the minimum period. This phase of the secular evolution is characterized by an almost constant mass transfer rate ($\ddot{M} \approx 0 \Rightarrow g_1$ large), depending almost solely on M_1. The spread in M_1 thus translates into the width of that maximum. The missing WDs between the low-mass He-WDs and the high-mass C/O-WDs in a realistic distribution of birth rates (Fig. 1) cause the central dip at $\log(\dot{M}/M_\odot \mathrm{yr}^{-1}) \approx -10.4$ in the maximum of model pm3, leaving two distinct peaks (the left one belonging to the He-WDs, as the dotted line in Fig. 5 indicates).

The linear part of $\log n$ for $\log(\dot{M}/M_\odot \mathrm{yr}^{-1}) \lesssim -10.6$, $\log n \propto -a \log \dot{M} + b$, $a \approx 1/2$, finally represents the secular evolution beyond the minimum period $P_{\min}$, where $\dot{M}$ rapidly decreases with time. Each contributing subdistribution g_1 discontinously drops to 0 at a smallest mass transfer rate characterizing the oldest CVs born $T_G = 10^{10}$ yr ago. The smooth edge of $n(\log \dot{M})$ near $\log(\dot{M}/M_\odot \mathrm{yr}^{-1}) \approx -12$ results from the dependence of this lower limit for $\dot{M}$ on $(M_{1,\mathrm{i}}, M_{2,\mathrm{i}})$.

4.3. Further intrinsic subdistributions

For completeness we show in Fig. 6 the intrinsic distribution of secondary masses for models pm1 and pm3, and list – without further discussion – some characteristic features of $n(\log M_2)$:

$\log(M_2/M_\odot) \approx$	
-0.3	local maximum due to bipolytrope model
-0.4371	limiting mass $M_{\mathrm{conv},0}$
-0.58	limiting mass M_{conv}, where secondaries of CVs born with large $M_{2,\mathrm{i}}$ become fully convective
-1.15	M_2 at minimum period $P_{\min}$

The remaining 1-dim. subdistribution $n(x)$ of the computed 4-dim. distribution $n(M_1, M_2, P, \dot{M})$ not yet discussed is the one of the WD mass. However, since we assume M_1 = const. throughout the evolution, the present intrinsic M_1-distribution is the same as the one of newborn CVs, i.e. $n(M_1) \propto \int b(M_{1,\mathrm{i}}, M_{2,\mathrm{i}})\, \mathrm{d}M_{2,\mathrm{i}}$. A representation of such a distribution can be found in DK (Fig. 7).

An interesting view on the 2-dim. subdistribution $n(\log P, \log \dot{M})$ for model pm3 over the $\log P$-$\log \dot{M}$-plane (Fig. 7), the preferred diagram in the context of secular evolution, concludes the discussion of the shape of various sub-

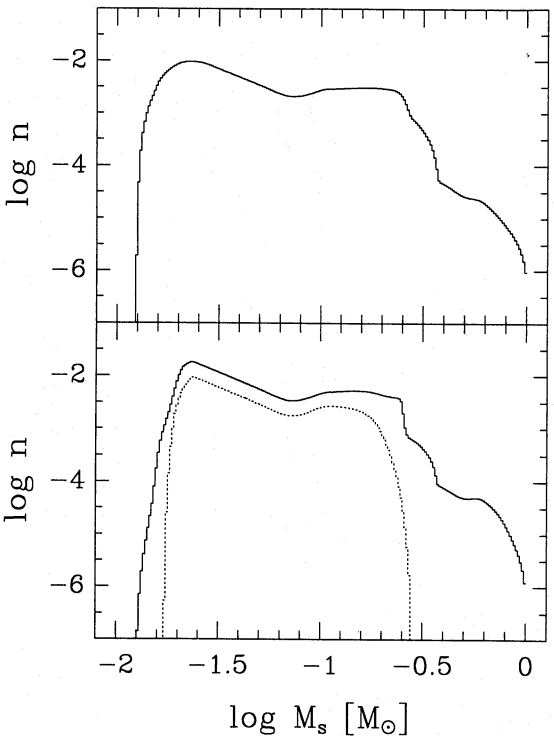

Fig. 6. The same as Fig. 5, but for the distribution function $n(\log M_2)$ of the secondary mass

distributions. It is instructive to compare this figure to Fig. 8, where evolutionary tracks of CVs in the $\log P$-$\log \dot{M}$-plane are shown, tracks along which the subsets of the present CV population with the corresponding $(M_{1,\mathrm{i}}, M_{2,\mathrm{i}})$-value are distributed.

4.4. Differential comparison of population models

In the following we investigate the influence of different CV formation rates (as tabulated in Table 1) and different MB-laws (Table 2) on the resulting CV population.

Table 3 summarizes the nine population models to be discussed below and lists relative "occupation numbers" N_i/N_Σ of various period intervals i. These intervals are defined with respect to the region $0.37 \lesssim \log(P/\mathrm{h}) \lesssim 0.51$ (enclosing the detached phase of CVs born with a $1M_\odot$ WD and high secondary mass), which we call – somewhat arbitrarily – the "period gap". It will turn out below that this interval is approximately the gap in the predicted observable period distribution. Hence, N_a denotes the number of CVs above the period gap (i.e. with $\log(P/\mathrm{h}) > 0.51$), N_b the number of CVs below the period gap ($\log(P/\mathrm{h}) < 0.37$), and N_in the number of (semi-detached!) CVs within the period gap ($0.37 \le \log(P/\mathrm{h}) \le 0.51$). The total number of CVs in the population model is thus $N_\Sigma = N_\mathrm{a} + N_\mathrm{in} + N_\mathrm{b}$. Finally, N_d denotes the total number of systems presently situated in the detached phase (N_d is not included in N_Σ).

In general, the occupation numbers obey roughly the relation

$$N_\mathrm{a} : N_\mathrm{in} : N_\mathrm{b} \approx 0.5 : 0.5 : 99 \,. \qquad (31)$$

Table 3. Summary of the population models; see text and Tables 1, 2 for further explanations. The last column gives an internal model number.

model	birth rate	MB-law	N_a/N_Σ	N_{in}/N_Σ	N_b/N_Σ	N_d/N_Σ	internal
pm1	bConst	VZtotal	0.0035	0.0093	0.9872	0.0266	D1/M003
pm2	maxM2	VZtotal	0.0105	0.0050	0.9845	0.0886	D-/M013
pm3	Pol	VZtotal	0.0047	0.0052	0.9901	0.0385	D2/M002
pm4	dK1	VZtotal	0.0045	0.0066	0.9889	0.0400	D3/M007
pm5	dK1in	VZtotal	0.0020	0.0074	0.9906	0.0186	D5/M009
pm6	dK03in	VZtotal	0.0021	0.0089	0.9890	0.0184	D6/M010
pm7	Pol	MS	0.0051	0.0052	0.9897	0.0396	D9/M006
pm8	Pol	JConst	0.0059	0.0052	0.9889	0.0400	D10/M012
pm9	Pol	VZConv	0.0087	0.0053	0.9860	0.0343	D8/M005

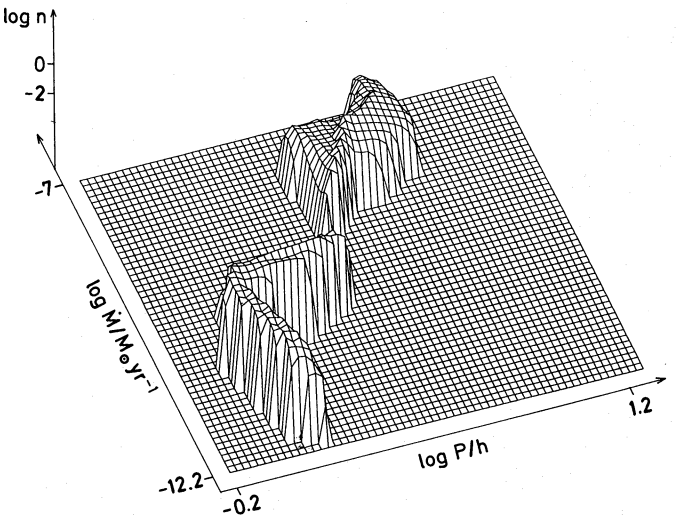

Fig. 7. The 2-dim. intrinsic distribution $n(\log P, \log \dot{M})$ over the $\log P$-$\log \dot{M}$-plane for model pm3 (see Table 3), not normalized

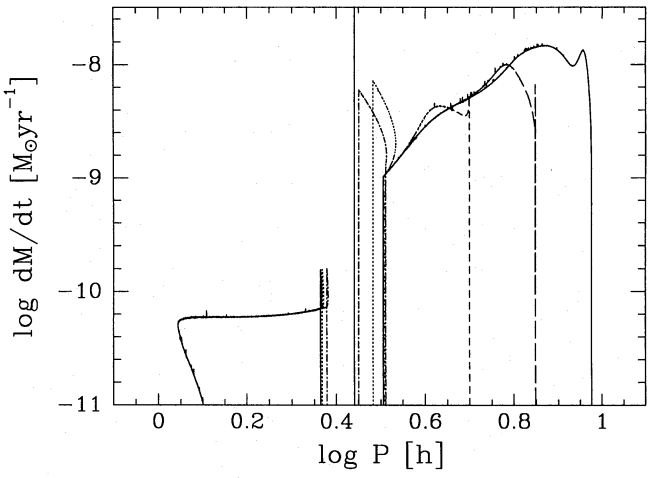

Fig. 8. Evolutionary sequences of CVs in the same plane as in Fig. 7, computed with Mazzitelli's stellar evolution code and assuming the MB-law VZtotal (M_1 = const. = $1.0M_\odot$). The sequences differ in the initial secondary mass (those with $M_{2,i} \leq 0.9M_\odot$ are already published in KR): $M_{2,i} = 1.2M_\odot$ (full line), $0.9M_\odot$ (long dashes), $0.6M_\odot$ (short dashes), $0.4M_\odot$ (dotted), $0.36M_\odot$ (dash-dotted). The vertical line at $P \approx 2.16$ h marks the critical period P_{crit}

For realistic population models N_d is on the order of a few percent ($N_d/N_\Sigma \approx 2-4\%$), and $\approx 70\%$ of all CVs are beyond the minimum period.

To account for the small ratio N_a/N_b we choose the following "scaled" representation of the resulting intrinsic distribution of orbital periods (the most important one in view of observational constraints, and thus the only one shown here for all population models; sometimes we use the notation n_{pmj} to address the period distribution of model pm$j$): we divide the period range at the critical period $\log(P_{crit}/h) = 0.4675$ and normalize the function n according to

$$\int n(\log P)\, d\log P = 1 \qquad (32)$$

in each part separately. In other words: above P_{crit} the function n is multiplied by a certain amplification factor $af > 1$ with respect to the normalization of n below P_{crit}. The value for af is given in the corresponding figure caption.

4.4.1. The influence of the birth rate

For reasons which will become obvious, we begin our discussion with a comparison between population models pm1 and pm2 (Fig. 9), which are based on the artificially chosen, very simple (but extreme) descriptions bConst and M2max for the CV formation rate (see Table 1). The period distribution of pm1, already discussed in Sect. 4.1 (Fig. 4, where it is shown on a logarithmic scale), is characterized by its overall very smooth shape (full line in Fig. 9). In contrast, model pm2 (dotted line) exhibits edges and small discontinuities, reflecting structures from individual subdistributions belonging to a fixed $(M_{1,i}, M_{2,i})$-value. These stand out so clearly because for each value of $M_{1,i}$ only *one* evolutionary sequence with $M_{2,i} = M_{2,max}(M_{1,i})$ contributes to the total distribution, and a comparatively coarse $M_{1,i}$-grid was used to generate model pm2.

The main differences between the models clearly arise from the lack of CVs with small initial secondary masses, in other words, from the relative dominance of high-mass CVs in pm2. Consequently, the period distribution of pm2 – when compared to pm1 – shows a larger ratio N_a/N_b (see Table 3) and is less concentrated above the period gap towards shorter periods. Moreover, below the period gap the "oldest" CVs are miss-

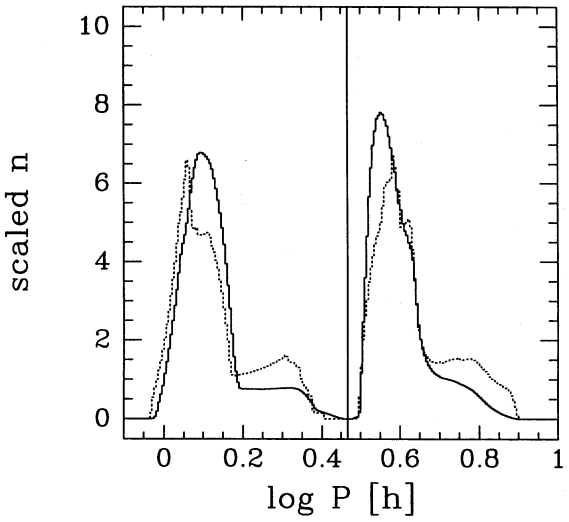

Fig. 9. The influence of the initial secondary mass spectrum: the scaled intrinsic period histogram for the population models pm1 (full line; af = 277; birth rate bConst) and pm2 (dotted; af = 93; birth rate M2max). A vertical line indicates the position of the critical period $\log(P_{\rm crit}/{\rm h}) = 0.4675$, the quantity af denotes the amplification factor for n above $P_{\rm crit}$ (see text for an explanation of the scaled plots)

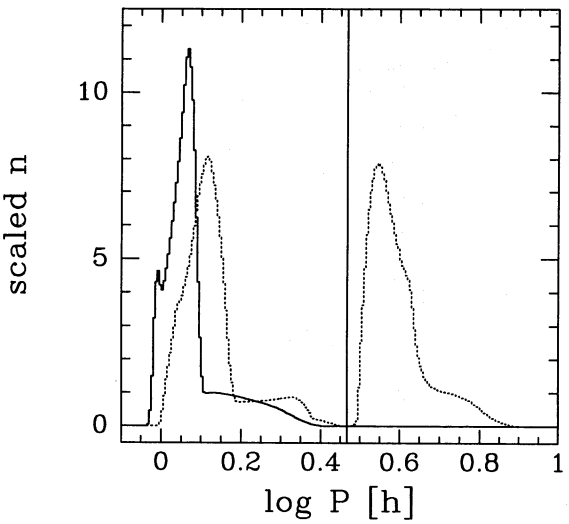

Fig. 10. The influence of the initial WD mass spectrum: the scaled intrinsic period distribution for certain subgroups of model pm1: CVs with $M_{1,\rm i} \leq 0.33 M_\odot$ (full line; af = 1) and CVs with $M_{1,\rm i} \geq 0.50 M_\odot$ (dotted line; af = 207). See also Fig. 9

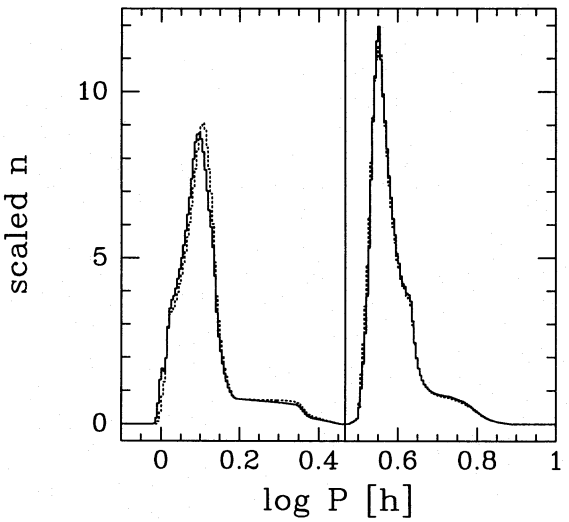

Fig. 11. The influence of $\alpha_{\rm CE}$: scaled intrinsic period distribution for model pm5 (full line; af = 501; $\alpha_{\rm CE}$ = 1) and model pm6 (dotted; af = 476; $\alpha_{\rm CE}$ = 0.3), see also Table 3 and Fig. 9

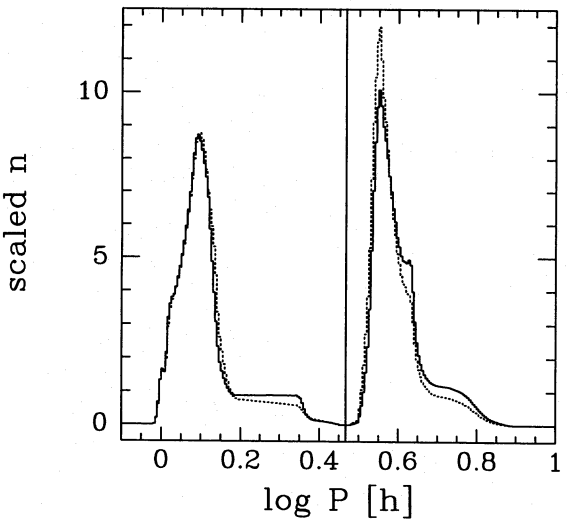

Fig. 12. The influence of the q_0-distribution: scaled intrinsic period distribution for model pm4 (full line; af = 219; q_0 = 1 preferred) and model pm5 (dotted; af = 501; independent choice), see also Table 3 and Fig. 9

ing, which now have the smallest secondary masses and which are responsible for the extension of the branch of $n(\log P)$ beyond $P_{\rm min}$ towards longer orbital periods. The local maximum of $n_{\rm pm2}$ at $\log(P/{\rm h}) \approx 0.3$ and the adjoining period interval $0.15 \lesssim \log(P/{\rm h}) \lesssim 0.30$ characterized by $\partial n_{\rm pm2}/\partial \log P > 0$ (as compared to $\partial n_{\rm pm1}/\partial \log P \approx 0$ in this region) result from the fact that there is a smallest allowed initial secondary mass in pm2, corresponding to the smallest WD mass where $b \neq 0$.

The extreme model populations pm1 and pm2 provide information about the influence of the initial *secondary mass* spectrum. In order to demonstrate the role of the initial *WD mass* spectrum Fig. 10 depicts two subdistributions of pm1: systems with low-mass WDs, $M_{1,\rm i} \leq 0.33 M_\odot$ ("He-WDs"; full line), and systems with high-mass WDs, $M_{1,\rm i} \geq 0.50 M_\odot$ ("C/O-WDs", dotted line). The former are not present above the period gap, since in that case the stability criterion forbids initial secondary masses $M_{2,\rm i} > M_{\rm conv,0}$. Below the period gap both groups leave clear signatures in the period distribution, above as well as beyond the period minimum: the branch above $P_{\rm min}$ is characterized by $\partial n/\partial \log P < 0$ and $\partial n/\partial \log P \gtrsim 0$ for low-mass and high-mass WDs respectively, whereas the broad peak of the branch beyond $P_{\rm min}$ is shifted towards longer or-

bital periods for high-mass WDs (i.e. larger values for $P_{\rm min}$, but also longer periods for the oldest CVs born 10^{10} yr ago and now far beyond $P_{\rm min}$). In the case of low-mass WDs the spike at $P_{\rm min}$ belonging to subdistributions for individual $M_{2,\rm i}$-values ($n \propto P/\dot{P} \rightarrow \infty$) remains visible in the integrated P-distribution.

We now turn to a more realistic prescription of the formation rate b and investigate in particular the influence of the CE parameter $\alpha_{\rm CE}$ and the initial q_0-distribution of the main-sequence binaries on our computed CV population.

Figure 11 depicts the P-distribution of model pm5 ($\alpha_{\rm CE}$ = 1, full line) and model pm6 ($\alpha_{\rm CE}$ = 0.3, dotted line), based on birth rate models dK1in and dK03in – see Tables 1 and 3. Obviously, the P-distribution is not sensitive to $\alpha_{\rm CE}$. The main consequence of reducing $\alpha_{\rm CE}$ is to reduce the number of He-WDs (see DK, Figs. 7c,d); hence a transition from pm5 to pm6 weakens the contribution of the subdistribution belonging to He-WDs and thus shifts the maximum of the branch of n beyond $P_{\rm min}$ towards longer orbital periods and increases (flattens, i.e. makes it less negative) the slope $\partial n/\partial \log P$ of the branch of n above $P_{\rm min}$, see Fig. 10 and the discussion above. This explains the marginal differences between pm5 and pm6 below the period gap.

Finally Fig. 12 attends to models pm4 (full line) and pm5 (dotted line) which differ in the initial q_0-distribution of main-sequence binaries (whereas both populations are computed with $\alpha_{\rm CE}$ = 1, see Table 3). As can be seen from Figs. 6a,c and 7a,c in DK, the main effect of changing the q_0-distribution from the case where q_0 = 1 is preferred (pm4) to the case with the independent choice of primary and secondary mass (pm5) concerns the resulting secondary mass spectrum of a newborn CV generation (the WD mass spectrum is much less sensitive): in the former case the CVs with high initial secondary mass dominate, in the latter the secondary masses are more uniformly distributed. This provides an immediate explanation for the differences between $n_{\rm pm4}$ and $n_{\rm pm5}$ – which are qualitatively the same as between pm2 and pm1 (Fig. 9), namely a larger ratio $N_{\rm a}/N_{\rm b}$, a less strongly concentrated distribution towards shorter periods above the gap, and a shift of the broad peak beyond $P_{\rm min}$ towards smaller P-values (when pm4 is compared with respect to pm5).

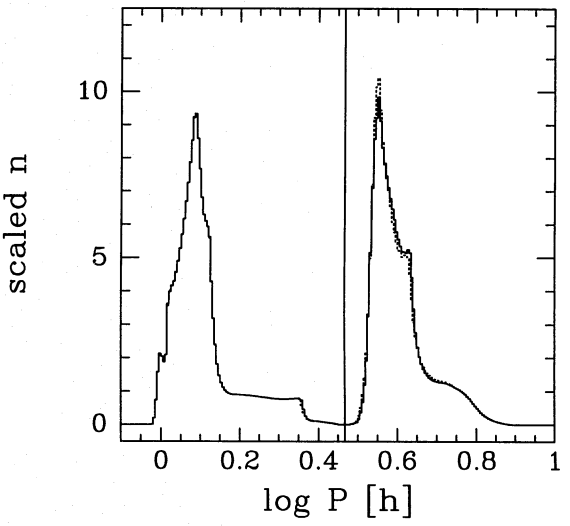

Fig. 13. The influence of the MB-law I: scaled intrinsic period distribution for model pm3 (full line; af = 212; MB-law VZtotal) and model pm7 (dotted; af = 193; MB-law MS), see also Table 3 and Fig. 9

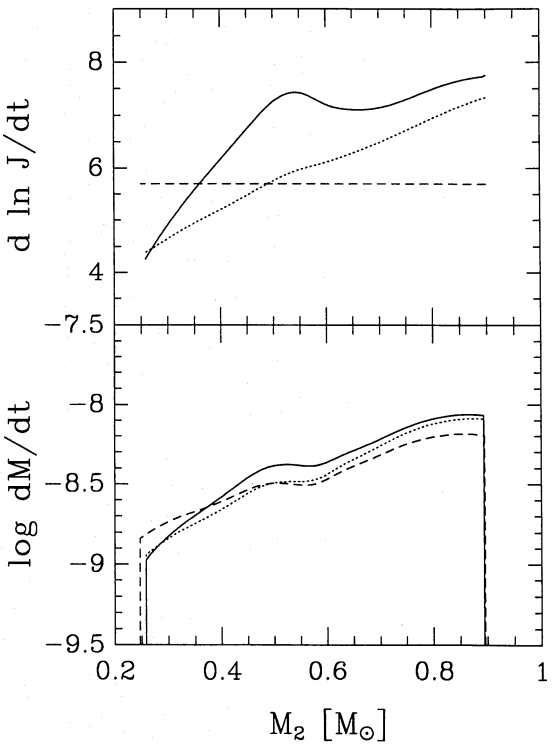

Fig. 14. Secular evolution with different MB-laws. The run of $|\dot{J}_{\rm MB}/J|$ (in $10^{-9}{\rm yr}^{-1}$; upper frame) and the mass transfer rate $\log \dot{M}$ (in $M_\odot{\rm yr}^{-1}$; lower frame) as a function of secondary mass M_2 (in $M_\odot$) for three different evolutionary sequences, computed with the bipolytrope code and based on different MB-laws (Table 2): VZtotal (full line), MS (dotted), JConst (dashed), as for models pm3, pm7 and pm8, respectively ($M_{1,\rm i}$ = $1.0M_\odot$, $M_{2,\rm i}$ = $0.9M_\odot$ for all sequences)

4.4.2. The influence of the magnetic braking law

The previous paragraph dealt with CV population models constructed by means of a "standard" prescriptions for computing $\dot{J}_{\rm MB}$, the Verbunt & Zwaan law with $f_{\rm VZ}$ = 1 (model VZtotal in Table 2). We now wish to compare four competing MB-laws and keep the birth rate b (model Pol, see Table1) fixed. This procedure introduces a minor inconsistency, since magnetic braking also enters the computation of the CV formation rate. However, numerical experiments show that changing the functional dependence of the angular momentum loss rate (within reasonable limits) has little effect on b (DK). In line with this finding is the close similarity of our population models pm3 (based on Poli-

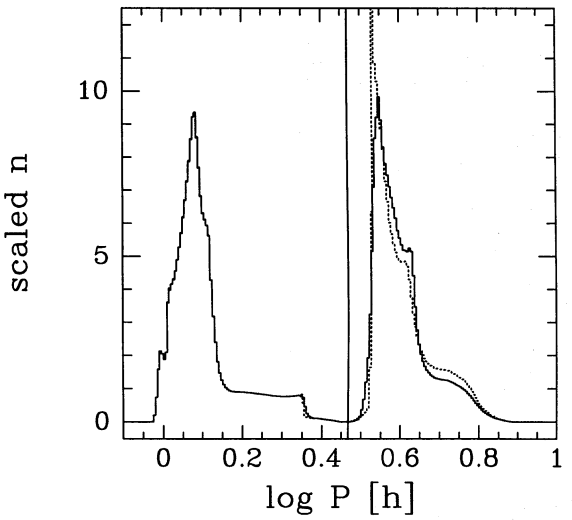

Fig. 15. The influence of the MB-law II: scaled intrinsic period distribution for model pm3 (full line; af = 212; MB-law VZtotal) and model pm8 (dotted; af = 167; MB-law JConst), see also Table 3 and Fig. 9

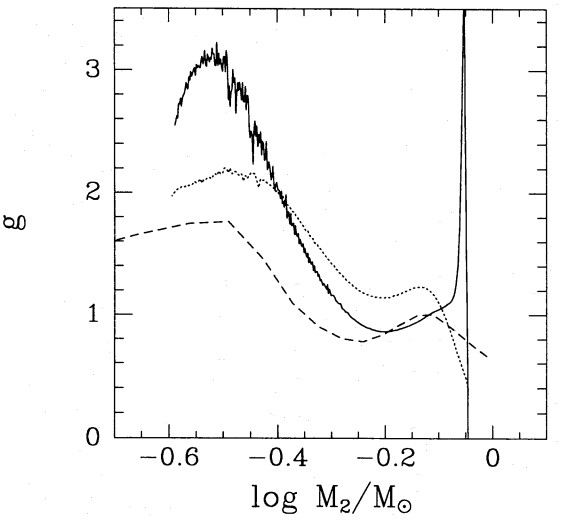

Fig. 17. The quantity g, defined in Eq. (35), as a function of secondary mass M_2 for the evolutionary sequences no. 1 (full line) and no. 5 (dotted) of KR. The dashed curve is obtained if g is computed with ζ_e instead of ζ_{eff} (see Fig. 16 and text)

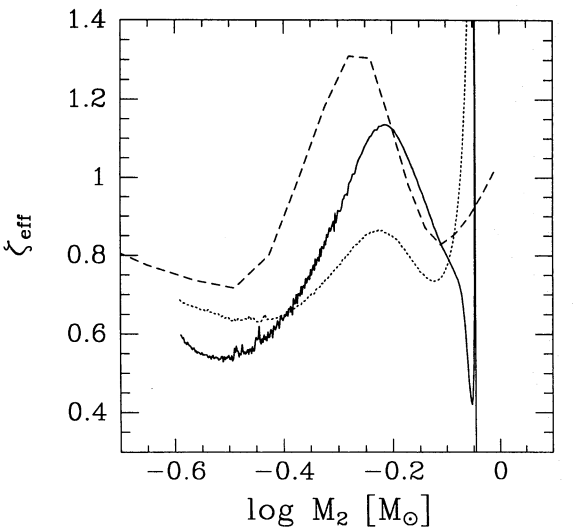

Fig. 16. The effective mass-radius exponent ζ_{eff} as a function of secondary mass M_2 for the evolutionary sequences no. 1 (full line) and no. 5 (dotted) of KR, where M_1 = $1.0M_\odot$, $M_{2,i}$ = $0.9M_\odot$, and the MB-law VZtotal and VZconv was assumed, respectively (oscillations reflect numerical noise). The dashed curve shows the mass-radius exponent ζ_e of the main sequence

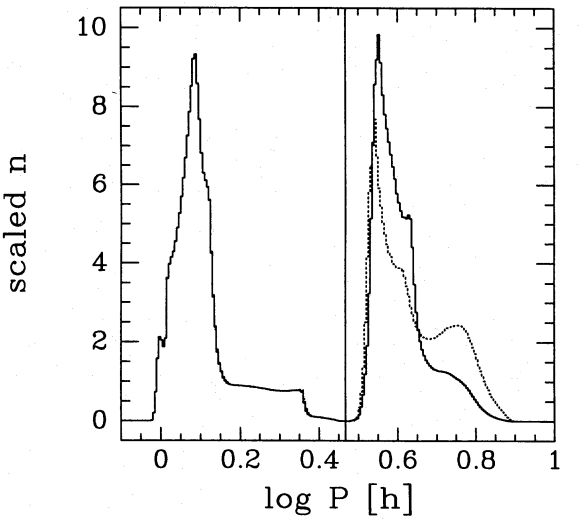

Fig. 18. The influence of the MB-law III: scaled intrinsic period distribution for model pm3 (full line; af = 212; MB-law VZtotal) and model pm9 (dotted; af = 113; MB-law VZconv), see also Table 3 and Fig. 9

tano's calculations) and pm4 (based on deKool's calculations, i.e. on a different MB-law, see Sect. 3.1).

Before resuming the discussion of P-distributions we stress that any differential comparison of CV evolution involving different MB-laws requires an adequate calibration of the MB-laws to each other. Since none of the former comparative studies in literature dealing with magnetic braking (the most recent one was Shafter 1992) paid any attention to that – in our opinion – important point, we formulate here one possible realization of the gauge process explicitely as a rule:

Choose the free parameters of the different magnetic braking prescriptions such that the corresponding evolution of a specific CV born with a sufficiently high secondary mass (e.g. with the highest allowed one) leads in each case to a detached phase as similar as possible (in extent and position) in period space.

In other words: changing the MB-law must preserve the values of P_l and P_u.

In our case, such a preparation results in the values of the free parameters listed in Table 2; the reference MB-law was the standard prescription according to Verbunt & Zwaan as quoted

above. This gives rise to a detached phase which is on average ($2.34 \lesssim P/\mathrm{h} \lesssim 3.24$) slightly too narrow in P and at too long orbital periods when compared to the observed period gap between 2 h and 3 h – a systematic difference *not* affecting our differential study; for a further discussion of this point see also Sect. 5.

We now turn to the surprising result depicted in Fig. 13: the MB-laws most often cited – according to Verbunt & Zwaan (1981; model pm3, full line) and Mestel & Spruit (1987; model pm7, dotted line) – lead to almost indistinguishable P-distributions when calibrated as described. Hardly any difference is detectable below the gap, above the gap n_{pm7} is slightly steeper towards P_{u}. The ratio $N_{\mathrm{a}}/N_{\mathrm{b}}$ is also very similar in both cases, with slightly more systems above the gap for pm7.

In view of this unexpected similarity it seems worthwhile to investigate the extreme case of a constant relative angular momentum loss rate, $\dot{J}_{\mathrm{MB}}/J = \mathrm{const.}$ (model pm8): Figure 14 shows the run of $\dot{J}_{\mathrm{MB}}/J$ and $\log \dot{M}$ as a function of the secondary mass for three evolutionary sequences which were used to calibrate the MB-laws to each other, and provides all essential informations needed to understand the differences between the scaled P-distributions of models pm3 (full line in Fig. 15) and pm8 (dotted line in Fig. 15). Below the gap n_{pm3} and n_{pm8} are almost identical, but above n_{pm8} is relatively larger for long periods (where $\dot{M}$ is smaller, see Fig. 14) and relatively smaller for shorter periods (where $\dot{M}$ is larger). The incline of n_{pm8} near P_{u} is much steeper, i.e. there are significantly less CVs in the "radiative part" of the period gap ($P_{\mathrm{crit}} < P < P_{\mathrm{u}}$) — a consequence of the initial phase with $\dot{P} > 0$ (see Sect. 4.1), which has a larger extent in period space for sequences of model pm8 (since $|\dot{J}/J|$ is larger for pm8 near P_{u}). In contrast, the average mass transfer rate is smaller for pm8 above the gap, i.e. the evolution is slower, so $N_{\mathrm{a}}/N_{\mathrm{b}}$ is larger as for pm3.

Moreover, model pm8 clearly demonstrates that the characteristic shape of the period distribution above the period gap, i.e. the two steep parts (where $|\partial n/\partial \log P|$ is large), interrupted by a plateau-like part around $\log(P/\mathrm{h}) \approx 0.7$ (with small $|\partial n/\partial \log P|$), is due to the structure of the secondary and its reaction to mass transfer, *not* to the specific MB-law (remember that the feature at $\log(P/\mathrm{h}) \approx 0.63$ is a numerical artefact). The plateau can be traced back to a similar structure in the P-subdistributions $g_1(\log P)$ belonging to subsets of CVs with the same initial masses $M_{1,\mathrm{i}}$, $M_{2,\mathrm{i}}$ (see Fig. 2), i.e. to a property of a secular evolution starting with ($M_{1,\mathrm{i}}$, $M_{2,\mathrm{i}}$). This point deserves further attention:

Assuming Roche geometry and $R = R_{\mathrm{R}}$, $\dot{R} = \dot{R}_{\mathrm{R}}$ (R and R_{R} are the secondary's radius and Roche radius, respectively) during the phase of mass transfer, the period derivative $\dot{P}$ is related to the orbital angular momentum loss rate $(\partial \ln J/\partial t)_{\dot{M}_2=0}$ according to

$$\frac{\dot{P}}{P} \approx \frac{3\zeta_{\mathrm{eff}} - 1}{\zeta_{\mathrm{eff}} - \zeta_{\mathrm{R}}} \left(\frac{\partial \ln J}{\partial t}\right)_{\dot{M}_2=0}, \tag{33}$$

where $\zeta_{\mathrm{eff}} := \mathrm{d}\ln R/\mathrm{d}\ln M_2$ denotes the effective mass-radius exponent of the secondary, and $\zeta_{\mathrm{R}} := \partial \ln R_{\mathrm{R}}/\partial \ln M_2$ the mass-radius exponent of the secondary's Roche radius. Equation (33) derives from Eq. (8) in Ritter & Kolb (1992), if the approximation

$$R_{\mathrm{R}} \approx \left(\frac{8}{81(1+q)}\right)^{1/3} a \tag{34}$$

(Paczyński 1971) for the Roche radius is used (a is the orbital distance), leading to the expression $F \approx (3\zeta_{\mathrm{R}} - 1)/2$ for the quantity F defined in Eq. (10) of Ritter & Kolb (1992).

Inserting Eq. (33) into Eq. (29) and taking note of the definitions $\tau_J := |\partial \ln J/\partial t|^{-1}$ and

$$g := \frac{\zeta_{\mathrm{eff}} - \zeta_{\mathrm{R}}}{3\zeta_{\mathrm{eff}} - 1} \tag{35}$$

we finally obtain for the period distribution of a CV subset characterized by one single ($M_{1,\mathrm{i}}$, $M_{2,\mathrm{i}}$)-value the expression

$$g_1(\log P) \propto g\,\tau_J\,. \tag{36}$$

Figures 16 and 17 plot ζ_{eff} and the quantity g as a function of the secondary mass for the evolutionary sequences no. 1 and 5 of KR, which were computed with Mazzitelli's full stellar evolution code — hence free from any numerical artefacts or shortcomings introduced by the bipolytrope description. Also shown (dotted line) is the run of ζ_{eff} and g when the simplest approach to describe the secular evolution of CVs is applied, namely the assumption that the secondary always obeys the main-sequence mass-radius relation — i.e when ζ_{eff} is replaced by the slope $\zeta_{\mathrm{e}} = (\mathrm{d}\ln R/\mathrm{d}\ln M)_0$ of the main sequence. It becomes apparent that the approximation $\zeta_{\mathrm{eff}} = \zeta_{\mathrm{e}}$ indeed reproduces the qualitatitive evolution – apart from the early phases subsequent to the turn-on of mass transfer. In particular, the characteristic intermediate plateau of $n(\log P)$ above the period gap (which is already present in g) results from the "hump" of $\zeta_{\mathrm{e}}(M)$ in the range $0.4 \lesssim M/M_{\odot} \lesssim 0.7$ (see Fig. 16), a feature which in turn is related to the influence of the dissociation of H_2-molecules in the outermost layers of the star (mentioned for the first time by Copeland et al. 1970).

At the end of this paragraph we turn to model pm9, the only one which is significantly different from our standard model pm3. The underlying modified Verbunt & Zwaan law (VZconv, see Table 2) has the remarkable property that $|\dot{J}_{\mathrm{MB}}/J|$ *increases* (slightly) with decreasing period (see Fig. 4 in KR), in contrast to all other MB-laws discussed previously. The resulting overall smaller mass transfer rate in the corresponding evolutionary sequences above the period gap explains the larger ratio $N_{\mathrm{a}}/N_{\mathrm{b}}$ and the significantly larger fraction of CVs at longer periods for pm9, i.e the flatter run of n_{pm9} above the gap (see Fig. 18). Again almost no difference between pm3 and pm9 is visible below the gap.

4.5. The observable period distribution

In this last paragraph we supplement the above presentation of models for the intrinsic CV population by a brief discussion of the considerable changes in the P-distribution when the principal effects of observational selection are taken into account by

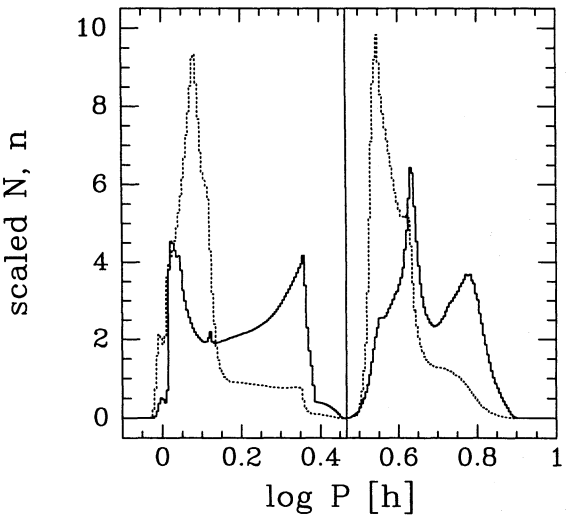

Fig. 19. Correcting for observational selection: the scaled observable period distribution $N(\log P)$ of model pm3 (full line; $af = 6.44\,10^{-2}$), computed with the selection factor Eq. (23), and the underlying intrinsic period distribution of pm3 (dotted; $af = 212$; MB-law VZconv), see also Table 3 and Fig. 9

Table 4. Occupation numbers for predicted observable distributions.

model	N_a/N_Σ	N_{in}/N_Σ	N_b/N_Σ
pm3	0.9346	0.0064	0.0590
pm6	0.8217	0.0212	0.1572
pm9	0.8921	0.0132	0.0948

multiplying the intrinsic distribution with the selection factor defined in Eq. (23). The application of a more detailed model for observational selection (an extension of the work by Ritter & Burkert 1986) and the comparative discussion of the resulting predicted observable distributions obtained from our different population models is outside the scope of this paper, but work on that is currently under progress (for first results see Dünhuber & Ritter 1992).

Figure 19 shows the observable period distribution $N(\log P)$ of model pm3 — as well as the corresponding uncorrected distribution n to facilitate the following comparison. The suppression of low-luminosity CVs (with small $\dot{M}$) in N leads to the disappearence of most systems beyond P_{min}; nevertheless, a peak near P_{min} remains, a feature which is clearly not present in the observed P-distribution.

The small spike at $\log(P/\mathrm{h}) \approx 0.12$ is a further numerical artefact of bipolytrope models and marks the transition between different approximations for intermediate and high degeneracy (see KR). Similarly, the property of the bipolytrope models connected with changes of the core's polytropic index (see Sect. 4.1) probably exaggerates the absolute maximum of N near $\log(P/\mathrm{h}) \approx 0.63$. The intermediate minimum of N in the range $0.65 \lesssim \log(P/\mathrm{h}) \lesssim 0.75$, on the other hand, seems to be a real feature, arising from the functional dependence of ζ_e on stellar mass discussed in the previous paragraph.

As can be seen from Fig. 19 the "period gap" of N is located between $\log(P_l/\mathrm{h}) \approx 0.37$ and $\log(P_u/\mathrm{h}) \approx 0.54$, i.e. is similar to the detached phase of systems with high initial secondary mass and a WD mass which corresponds roughly to the mean WD mass of the underlying formation rate model. The population density of the gap is smaller (but non-vanishing) to the right of P_{crit}, and smallest in the vicinity of P_{crit} (in our case $\log(P_{crit}/\mathrm{h}) = 0.4675$). The descending part of N at P_l is somewhat steeper than the rising part at P_u.

As far as the occupation numbers of the different period regimes are concerned (Table 4), our simple approach for observational selection predicts too many CVs situated above the gap ($N_a/N_\Sigma \approx 80\% - 90\%$), but the correct order of magnitude for those to be found within the gap ($N_{in}/N_\Sigma \approx 0.5\% - 2\%$).

5. Discussion and conclusions

Based on models for CV formation rates by DK and Politano (1988), and on the generalized bipolytrope description for the secular evolution of CVs (KR), we could for the first time synthesize fully self-consistent models describing the total CV population. The derived distribution functions for orbital period, mass transfer rate, secondary mass and WD mass refer to the *intrinsic* CV population, not to the ensemble of CVs we actually observe. The prediction of such observable distributions would require to correct the intrinsic distributions for observational selection effects, which is the topic of a forthcoming paper. In order to decide about the importance of the still free or little-known parameters within the theories describing the formation and evolution of CVs it is (in principle) necessary to investigate how these affect the predicted observable distributions. Nevertheless, our study shows that some firm results can already be drawn from their influence on the intrinsic distributions.

Our main results can be summarized as follows:

1) Intrinsically we find $\approx 99\%$ of all CVs below the period gap ($\approx 70\%$ beyond the minimum period), a number which is expected to be of that order, since the ratio of evolutionary time scales

$$\frac{\tau_{GR}}{\tau_{MB}} \approx 10 \ldots 100 \qquad (37)$$

below and above the gap is large. The remaining 1% fall in two, roughly equal parts, distributed within and above the period interval of the gap, respectively.

2) The ratio of the number of systems which are at present in the detached phase (crossing, invisible to us, the gap) to the total number of CVs amounts to only about $2\% - 4\%$.

3) The intrinsic CV population is not sensitive to the description of the CE-phase (i.e. to the parameter α_{CE}), whereas changes in the initial distribution of mass ratios of newly forming main-sequence binaries (from which CVs descend) influences noticeably the ratio of CVs above/below the gap as well as the shape of the resulting distribution functions.

4) It turns out that the shape of the intrinsic distribution above the gap is determined mainly by the secondary's stellar structure, the MB-law is only a "second order" effect. As long

as competing MB-laws do not differ drastically there seems to be little hope to decide about the precise functional dependence of $\dot{J}_{\rm MB}$ on sysytem quantities from a comparison with the observed period histogram. Although the fairly different prescriptions VZtotal (see Table 2), where the relative orbital angular momentum loss rate $|\dot{J}_{\rm MB}/J|$ decreases with decreasing orbital period, and VZconv, where $|\dot{J}_{\rm MB}/J|$ increases with decreasing P, should be distinguishable, the more realistic MB-laws according to Verbunt & Zwaan (1981) – VZtotal – and Mestel & Spruit (1987) lead, when calibrated adequately to each other (see the extended discussion in Sec. 4.4.2), to almost the same intrinsic populations, actually very similar to the one computed assuming a constant value for $|\dot{J}_{\rm MB}/J|$.

In this context we wish to comment on the work of Shafter (1992), who tried to test the Verbunt & Zwaan and Mestel & Spruit MB-laws by comparing the predicted ratio of dwarf novae to nova-like systems as a function of orbital period with the observed one. However, his underlying model of secular evolution, the assumption of a strict mass-radius relation for the secondary throughout the evolution, cannot account for deviations from thermal equilibrium and is thus unable to reproduce a "period gap" in a self-consistent way. Rather, Shafter assumed ad hoc a gap between 2 h and 3 h, without recognizing the necessity to calibrate the MB-laws to each other (see Sect. 4.4.2). Nevertheless, the main conclusions of Shafter's work – the impossibility to distinguish at present between these MB-laws – remains valid also after our more detailed analysis.

When discussing magnetic braking we further have to mention the recent paper by Tout & Pringle (1992) about the spin-down of rapidly rotating, convective stars. The authors developed a fully self-consistent picture of a magnetic dynamo, generated by differential rotation and convection, giving rise to a magnetically controlled stellar wind, which in turn causes a spin-down. The considerations of Tout & Pringle are in principle applicable to the CV case, although they refer to fully convective stars and thus are in conflict with our explanation of the period gap (it is not immediately clear how their results can be generalized for stars with a radiative core). However, this contradiction is toned down in view of the fact that the authors' expression (7.3) for $\dot{J}_{\rm MB}$ contains still one completely free parameter γ, measuring the efficiency of the regeneration term in the dynamo equations. Moreover, Tout and Pringle themselves point out that the details of the functional dependence of $\dot{J}_{\rm MB}$ should not be overrated with regard to the poorly understood physical processes entering. After all, the MB-law proposed by Tout & Pringle, though representing a promising new picture in itself, does not improve our understanding of the secular evolution of CVs.

Before we proceed to the next point of our main results, the discussion of the predicted observable period distribution, it seems worthwhile to take a critical look at some basic simplifications which we used to obtain the CV population models.

First, we assumed that the WD mass does not change when the systems evolve, a restriction which facilitated our computations since it reduces the multi-dim. intrinsic distribution function Eq. (10) by one order. Although observations and theoretical predictions drawn from thermonuclear runaway models for classical novae indicate that the WD mass can neither grow nor shrink substantially in the long-term mean (the observed chemical composition of nova envelopes shows that $\dot{M}_1 < 0$ in many cases), there is still considerable uncertainty about this point. It is related to the question of a CE-phase during nova explosions (see e.g. Livio et al. 1990; Shankar et al. 1991; Kato & Hachisu 1991) and of diffusion and mixing of core material into the envelope of the WD (see e.g. Iben et al. 1991; Shankar et al. 1992) and thus topic of a number of recent investigations. Hence, to allow for a changing WD mass is a desirable extension of our population synthesis.

The second important simplification in our approach concerns the neglect of any time dependence of the CV formation rate b. In reality we expect $\partial b/\partial t \neq 0$, since a) the star formation rate in our galaxy may have changed with history — observations and models for the chemical evolution of our galaxy indicate the occurence of an initial star formation burst (see e.g. Rana 1991; Burkert 1992) —, and b) even with an underlying constant star formation rate b would be time-dependent: the time interval between the formation of a main-sequence binary and its possible later appearance as a CV is a function of the initial binary parameters. The CV birth rate data computed by DK contain information about the time dependence due to the latter effect (see Figs. 8a, b of DK), but we omitted these for the time being to avoid the extension of our input tables into a third dimension.

The third simplification, the restriction to CVs with an initial secondary mass $\leq 1M_\odot$ due to limitations of the bipolytrope description, represents a more difficult problem. The direct consequence – our models exclude $\sim 20\%$ of the total CV population – is not as severe as it may seem at a first glance: Fig. 8 and former investigations (Sect. 3.2 in KR) show that evolutionary tracks of CVs born with high initial secondary mass converge to a common track in the characteristic evolution diagram combining orbital period and mass transfer rate. Accordingly, systems with $M_{2,\rm i} > 1M_\odot$ would evolve in a well-known way and the majority of them should add up to the intrinsic distributions presented in Sect. 4 for periods $\lesssim 8$ h without changing much. Only the youngest of them would populate the period regime above ~ 8 h, about which thus no detailed information can be given. However, this reasoning ignores the fact that for the CVs in question the secondaries are expected to be slightly evolved: with increasing stellar mass the nuclear timescale becomes shorter and eventually non-negligible against the pre-CV evolution timescale. Such evolved stars can no longer be approximated by the simple generalized bipolytrope description calibrated to the homogenous ZAMS (see KR) and require full stellar evolution computations. Work on this is under progress (Singer, Kolb & Ritter, in preparation).

Finally it should be noted that our models do *not* reproduce precisely position ($P_{\rm l}^o \approx 2$ h) and width ($P_{\rm u}^o - P_{\rm l}^o \approx 1$ h) of the observed period gap and the observed value $P_{\rm min}^o \approx 80$ min for the minimum period. Rather, the gap in our predicted observable P-distribution is located at too long orbital periods ($P_{\rm l} \approx 2.3$ h)

and is slightly too wide ($P_u - P_l = 1.1$ h); P_{min} is too small ($P_{min} \approx 65$ min). This mismatch does not affect our differential study of population models, which was not designed to achieve a perfect agreement (remember that our reference MB-law VZtotal was used with the "standard" strength $f_{VZ} = 1$, disregarding the consequences for the resulting detached phase in the evolution of a CV). On the other hand there is indeed a difficulty in adjusting the position *and* the width in period of the detached phase at the same time. Changing the strenth of magnetic braking above the gap influences not only P_u, but also the convective limiting mass M_{conv} and thus P_l; changing the functional dependence of MB (with fixed strength, i.e. fixed adequately chosen average $\langle \dot{J}_{MB}/J \rangle$) has only little effect. An additional parameter is needed, namely changing the limiting mass $M_{conv,0}$ for ZAMS stars. As e.g. Hameury (1991) has shown, this mass depends on input physics of the stellar structure.

Some authors introduce a further free parameter by allowing for a certain (small) amount of magnetic braking also below the period gap, i.e. for fully convective stars (see e.g. Hameury et al. 1990 and 1991). This cannot influence P_u, but – in principle – P_l: if $|\dot{J}_{GR}| + |\dot{J}_{MB}|$ is large enough and thus the shrinkage of the orbit during the detached phase fast enough, the secondary may not have reached thermal equilibrium yet when mass transfer resumes. The thus larger radius of the secondary at turn-on would cause a larger value for P_l as well. However, there are indications that magnetic braking is unimportant below the period gap (at least for AM Her stars, see Ritter & Kolb 1992).

The value of P_{min}, on the other hand, depends strongly on low-temperature opacities ($T \lesssim 2\,10^3$ K) in the outer layers of the secondary, hence the considerable uncertainties of the latter propagate into a similar uncertainty of the former (see e.g. Rappaport et al. 1982). The orbital angular momentum loss rate has only a little influence ($P_{min} \propto \dot{J}^{0.151}$ according to Paczyński & Sienkiewicz 1981, 1983), but a systematic increase of P_{min} is found if corrections for rotational and tidal deformation of the secondary are taken into account (see Nelson et al. 1985, where P_{min} increases by $\approx 10\%$ because of these corrections).

Despite all these simplifications and uncertainties of the underlying models our synthesized CV population yields a qualitatively and quantitatively reasonable prediction for the observable period distribution of a magnitude-limited sample of CVs, taken from a homogenously distributed CV population in physical space (Fig. 19), an overall very satisfying result. This turns us back to the summary of our main results, which we continue with the discussion of the fifth and last point:

5) The population synthesis shows that the disruption of magnetic braking, responsible for the detached phase of individual CVs, leads indeed to a pronounced "period gap" in the period distribution of the complete CV population – an inference always assumed to be correct, but never proved explicitely before. In other words: CVs born in the gap do not fill the gap. We find a fraction of 0.5% – 2% of all CVs in the gap, a value consistent with observations. Our result is also much more reliable than previous crude estimates, see e.g. DK. Moreover, concerning the location and its width, the resulting period gap is comparable to the detached phase in period space of CVs born with high $M_{2,i}$ and some mean value for $M_{1,i}$ ($\approx 0.7 M_\odot$).

In contradiction with observations, however, is the resulting large fraction (80% – 90%) of CVs above the period gap (this finding favours the independent choice of primary and secondary mass in the initial main-sequence binary, since the corresponding birth rate models give the lowest value for that fraction), and the spike at P_{min} visible in $N(\log P)$, Fig. 19, which is not present in the observed period histogram (see e.g. Ritter 1990). Preliminary results from more refined models considering a sample of CVs limited by the visual (instead of the bolometric) luminosity indicate that the discrepancy for long-period systems disappears, whereas the problem near P_{min} remains.

More detailed models will have to show whether our very simple description of observational selection is insufficient, or whether we still lack an essential ingredient in our intrinsic population models, e.g. in the understanding of the secular evolution of CVs. A closer investigation of possible fluctuations of the mass transfer rate $\dot{M}$ on short time scales (as it was suggested to explain the spread in the observed values of $\dot{M}$ at a given orbital period, see e.g. Warner 1987, Patterson 1984 and the discussion in Hameury et al. 1989) and of the consequences of the expected CE phase during nova-explosions (i.e. the frictional orbital angular momentum losses, see Livio et al. 1991) may be interesting in this context.

Acknowledgements. The author would like to thank Dr. H. Ritter for initiating this work and for valuable advice, Drs. M. deKool and M. Politano for providing their data on CV formation rates, and Dr. J. Brown for improving the language of the manuscript.

References

Burkert, A., 1992, J. Phys. G, in press
Copeland, H., Jensen, J.O., Jørgensen, H.E., 1970, A&A, 5, 12
Dünhuber, H., Ritter, H., 1992, in *White Dwarfs: Advances in Observations and Theory*, ed. M.A. Barstow, NATO ASI-Series, Kluwer, Dordrecht, in press
Hameury, J.M., 1991, A&A, 243, 419
Hameury, J.M., King, A., Lasota, 1989, MNRAS, 237, 39
Hameury, J.M., King, A., Lasota, 1990, MNRAS, 242, 141
Hameury, J.M., King, A., Lasota, 1991, A&A, 248, 525
Hameury, J.M., King, A., Lasota, J.P., Livio, M., 1989, MNRAS, 237, 835
Hameury, J.M., King, A., Lasota, J.P., Ritter, H., 1988, MNRAS, 231, 535
Hjellming, M.S., 1989, *PhD thesis*, University of Illinois, Urbana-Champaign
Iben, I., Jr., Fujimoto, M.Y., MacDonald, J., 1991, ApJ, 375, L27
Kato, M., Hachisu, I., 1991, ApJ, 373, 620
King, A.R., 1988, QJRAS, 29, 1
Kolb, U., Ritter, H., 1992, A&A, 254, 213 (KR)
deKool, M., 1992, A&A, 261, 188 (DK)
Kraft, R.P., Mathews, J., Greenstein, J.L., 1962, ApJ, 136, 312
Livio, M., Govarie, A., Ritter, H., 1991, A&A, 246, 84
Livio, M., Shankar, A., Burkert, A., Truran, J.W., 1990, ApJ, 356, 250
Mazzitelli, I., 1989, ApJ, 340, 249

Mestel, L., Spruit, H.C., 1987, MNRAS, 226, 57
Nelson, L.A., Chau, W.Y., Rosenblum, A., 1985, ApJ, 299, 658
Paczyński, B., 1971, ARA&A 9, 183
Paczyński, B., 1976, in *IAU Symp. Nr. 73: Structure and Evolution of Close Binary Systems*, ed. P. Eggleton, S. Mitton, J. Whelan, Reidel, Dordrecht, p. 75
Paczyński, B., Sienkiewicz, R., 1981, ApJ, 248, L27
Paczyński, B., Sienkiewicz, R., 1983, ApJ, 268, 825
Patterson, J., 1984, ApJS, 54, 443
Politano, M., 1988, *PhD thesis*, University of Illinois, Urbana-Champaign
Politano, M., 1990, in *Accretion-Powered Compact Binaries*, ed. C.W. Mauche, Cambridge University Press, Cambridge, p. 421
Rana, N.C., 1991, ARA&A, 29, 129
Rappaport, S., Joss, P.C., Webbink, R.F., 1982, ApJ, 254, 616
Rappaport, S., Verbunt, F., Joss, P.C., 1983, ApJ, 275, 713
Ritter, H., 1990, A&AS, 85, 1179
Ritter, H., 1991, in *High Energy Astrophysics: Compact Stars and Active Galaxies*, ed. Li Quibin, World Scientific Publ. Co., Singapur, p. 107
Ritter, H., Burkert, A., 1986, A&A, 158, 161
Ritter, H., Kolb, U., 1992, A&A, 259, 159
Ritter, H., Politano, M., Livio, M., Webbink, R.F., 1991, ApJ, 376, 177
Shafter, A.W., 1992, ApJ, 394, 268
Shankar, A., Arnett, D., Fryxell, B.A., 1992, ApJ, 394, L13
Shankar, A., Livio, M., Truran, J.W., 1991, ApJ, 374, 623
Spruit, H.C., Ritter, H., 1983, A&A, 124, 267
Tout, C.A., Pringle, J.E., 1992, MNRAS, 256, 269
Verbunt, F., Zwaan, C., 1981, A&A, 100, L7
Warner, B., 1976, in *IAU Symp. No. 73: Structure and Evolution of Close Binary Systems*, eds. P. Eggleton, S. Mitton, J. Whelan, Reidel, Dordrecht, p. 85
Warner, B., 1987, MNRAS, 227, 23

This article was processed by the author using Springer-Verlag LaTeX A&A style file version 3.